POLITECNICO DI MILANO
Dottorato di Ricerca in Ingegneria Strutturale, Sismica e Geotecnica
Ph.D. Degree in Structural, Seismic and Geotechnical Engineering

XXVI Ciclo

The Influence of Cardiac Trabeculae on Ventricular Mechanics

Tesi di Dottorato dell'Ing. Marta Serrani

Tutor:
Prof.ssa Maria Laura Costantino

Coordinatore:
Prof. Roberto Paolucci

Relatori:
Prof.ssa Maria Laura Costantino
Prof. Roberto Fumero

March 2014

Alla mia famiglia,

A Francesco.

Abstract

Cardiac trabeculae are cylindrical structures characterized by an axial orientation of myocytes which cover the inner surfaces of both ventricles. They are arranged in a complex shape, but preferably oriented along the ventricular apico-basal direction. The trabeculae represent a significant percentage of ventricular mass (12%-17%), and a value of trabecular mass higher than 20% is considered an index of pathology. The aim of the thesis is to understand the role of trabeculae on heart performances. A finite-element model of the left ventricle was developed to simulate the cardiac cycle (Abaqus$^®$ 6.10, SIMULIA, Dassault Systémes). To compare different models (with or without trabeculae) the ventricle was simplified as a truncated ellipsoid and the trabeculae, if present, as cylindrical strands laying onto the endocardium oriented along the ventricular axis. Different trabeculae diameters and mass were implemented to investigate the influence of these parameters on the model outcomes. The total muscular mass and the intra-ventricular volume were kept constant in all models.

The cardiac tissue mechanical behaviour was modelled by an anisotropic hyperelastic law. The material parameters were optimized to fit the physiologic pressure-volume relationship during the diastole. Cardiac fibres were oriented helically in the ventricular wall and along the axial direction in the trabeculae, according to the literature. The muscular contraction was simulated by increasing the material stiffness according to the contraction curve of a cardiac fibre secondary to an intracellular calcium variation. To avoid any rigid motions of the structure, kinematic boundary conditions were applied at the ventricular base. Physiologic atrial pressure was set during the ventricular filling phase, while an adequate RCR model was connected downstream to the ventricle to simulate the systemic circulation. The results show a significant difference in the ventricular hemodynamic if the trabeculae are present. The trabeculated model is characterized by an higher compliance with respect to the "smooth" model. Besides, the end-diastolic volume and the stroke volume increase with the trabecular mass, while the trabeculae diameter influences the fibre stress distribution. The ventricular filling is

_____

a fundamental parameter in heart functioning; more than the 50% of the patients suffering of heart failure symptoms show a normal ejection fraction and are referred to as diastolic heart failure patients. In this context, the trabeculae can play a fundamental role, since they significantly contribute to the achievement of a physiologic end-diastolic volume and, consequently, a physiologic cardiac output. Furthermore, the myocardial oxygen consumption depends on the cardiac frequency. Since the trabeculated ventricle is able to guarantee a physiologic cardiac output at lower heart rate with respect to the smooth ventricle, these results encourage further studies to investigate a possible enhanced ventricular efficiency determined by the presence of trabeculae at the endocardium.

_____

Acknowledgments

My first thanks go to my supervisors Prof. Roberto Fumero and Prof. Maria Laura Costantino for their interest in my work and their constant mentoring. With their experience, advices and enthusiasm they push me to give my best.

I am also very grateful to Prof. Marcello Gambacorta (Ospedale Niguarda, Milan) and Prof. Gabriele Guidi (Mechanical Engineering Department, Politecnico di Milano) for their help and for the interest they have demonstrated for this research.

Special thanks to former and present members of my research group, for helping me to reach my objectives, but also for the amazing time we spent together. A special mention to Massimiliano, whose contribution was fundamental for the realization of this work. I sincerely thank all the members of LaBS - professors, researchers, students - for their friendship, sympathy, and understanding. They have contributed to make this experience special, sharing with me joys and sorrows. It was an honour to be part of it.

I'd like to extend my gratitude to Dr. Geoff Moggridge for the patience he showed while I finished writing this thesis during my first "post-doctoral" research position at Cambridge University.

Many thanks to all my dearest friends for always being there, no matter what.

I owe a great deal to my parents and my brother, for their unfailing support, and to all my family: without you, this work wouldn't have been possible.
Finally, I owe so very much to Francesco, who really shared every moment of this hard journey with me …simply, thank you.

Marta

_____

Contents

_____

_____

Glossary of acronyms

bpm	beats per minute
CAD	Computer Aided Design
CO	Cardiac Output
DT-MRI	Diffusion Tensor Magnetic Resonance Imaging
EDV	End-Diastolic Volume
ESV	End-Systolic Volume
LVNC	Left Ventricular Non Compaction
PV	Pressure-Volume
PVA	systolic Pressure-Volume Area
TTI	Tension-Time Index

_____

Chapter 1 : INTRODUCTION

THE CARDIAC TRABECULAE

The trabeculae carneae are finger-like muscular structures which cover the endocardial surfaces of both the right and the left ventricles in the heart. In fact, they divide the heart wall into two different layers: a compact layer and a "spongy" layer. In this chapter an introduction about these particular structures will be given.

_____

1.1. ANATOMY AND STRUCTURE

The primary function of the heart is to pump blood into the circulatory system. The heart is composed of four chambers: the right and left atria, which receive blood from the body through the veins, and the right and left ventricles, which pump the blood into the pulmonary and systemic circulation through the arteries.

Atria and ventricles are separated by the atrio-ventricular valves: the mitral valve, placed between the left atrium and the left ventricle, and the tricuspid valve, which separates the right atrium and the right ventricle. Other two valves, called semi-lunar valves, regulate the blood ejected by the ventricles: the aortic valve which allows the blood to flow from the left ventricle towards the aorta, and the pulmonary valve which allows the blood to flow from the right ventricle to the pulmonary artery. All the cardiac valves open and close passively depending on the pressure difference acting on the valve; their correct functioning is fundamental to ensure a unidirectional blood flow in the circulatory system.

The heart is a pulsatile pump, and the cardiac cycle consists of two phases: a phase in which the ventricles are filled by blood, namely the cardiac diastole, and a period of blood ejection, the cardiac systole. During diastole the blood flows from the atria into the ventricles, thus inducing the passive ventricular filling. Subsequently, the ventricles contract, increasing the intra-ventricular pressure and allowing the blood to be ejected towards the arteries. A physiologic filling of the ventricles is crucial to guarantee an adequate cardiac output (CO); according to the Frank-Starling law, the contractile force of myocytes depends on their stretch during the diastolic phase (preload): the higher the ventricular volume at the end of the diastole (end-diastolic volume, EDV), the higher the ejected blood volume (stroke volume, SV).

The nourishment of all the cardiac cells is supplied by the coronary circulation, which originates from the aortic root and empties in the right atrium (Figure 1.1) [1].

Left pulmonary veins
Posterior cusp of mitral valve
Anterior (aortic) cusp of mitral valve
Aortic sinus (of Valsalva)
Right superior pulmonary vein
Left semilunar cusp of aortic valve
Ascending aorta
Posterior semilunar (non coronary) cusp of aortic valve
Superior vena cava
Atrioventricular part of membranous septum
nterventricular part of nembranous septum
Right atrium
Anterior cusp of tricuspid valve (retracted)
Septal (medial) cusp of tricuspid valve
Posterior cusp of tricuspid valve
Right ventricle
Right anterior papillary muscle (cut)
Right posterior papillary muscle
Muscular interventricular septum
Left ventricle
Left posterior papillary muscle

Left auricle
Left atrium
Pulmonary trunk
Ascending aorta
Openings of coronary arteries
Right auricle
Left semilunar cusp of aortic valve
Right semilunar cusp of aortic valve
Supraventricular crest
Outflow to pulmonary trunk
Conus arteriosus
Right anterior papillary muscle (cut)
Right ventricle
Moderator band of septomarginal trabecula
Septal band of septomarginal trabecula
Septal (medial) papillary muscle
Left ventricle
Left anterior papillary muscle
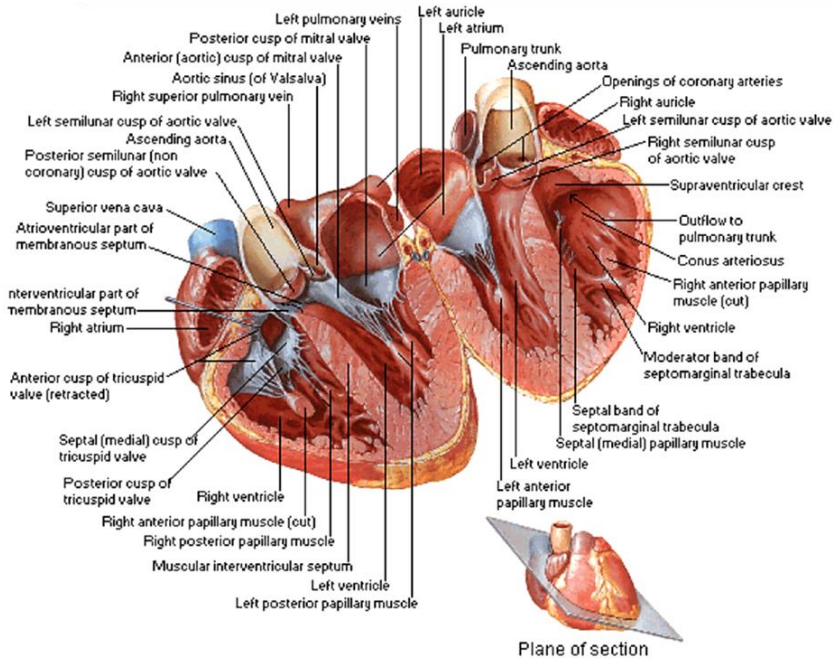
Plane of section

Figure 1.1. Human heart anatomy [2].

The curve which describes the intra-ventricular pressure change against the intra-ventricular volume variation during the cardiac cycle represents the pressure-volume relationship (or PV loop) of the ventricle. The PV loop provides fundamental information about the ventricular performances, highlighting alterations in the ventricular load conditions and pointing out the presence of different cardiac pathologies. An example of a physiologic PV loop of the left ventricle is shown in Figure 1.2; the most significant events which occur during the cardiac cycle are also described. The PV loop of the right ventricle is characterized by the same trend with respect to the left ventricular PV loop, but lower values of the ventricular pressure during the ejection phase. The PV loop area represents the work spent by the ventricle to eject the blood into the systemic circulation.
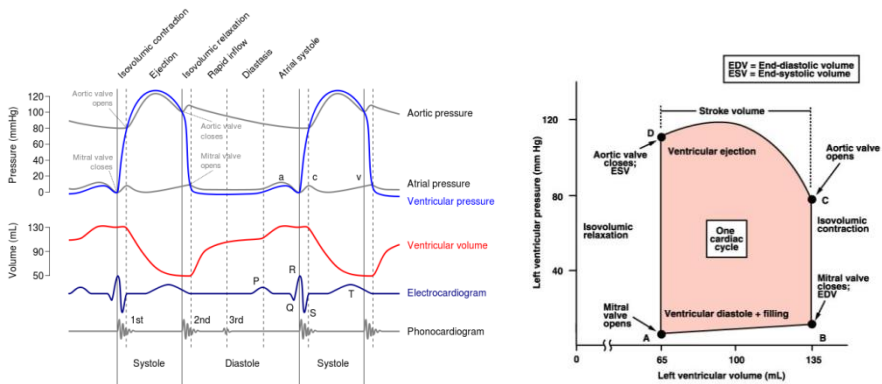
_____

Figure 1.2. Left: the Wiggers diagram shows the left ventricular pressure and volume courses during the cardiac cycle. The aortic and atrial pressure, the electrocardiogram and phonocardiogram curves are also shown [1]. Right: Schematic representation of a physiologic PV loop of the left ventricle. The different phases of the cardiac cycle are indicated: the ventricular filling phase (A-B), the isovolumetric contraction (B-C), the ejection phase (C-D) and the isovolumetric relaxation (D-A).

The inner surfaces of all heart chambers are covered by finger-like structures arranged in a complex network; in the right and left ventricle these muscular structures are known as *trabeculae carneae*. The trabeculae preferably arise from the free wall, namely the portion of the ventricular wall which is not in contact with the inter-ventricular septum, and insert into the atrio-ventricular ring [3]; thus, the trabeculae are mainly oriented along the apico-basal direction, but they can be found in almost any location within either ventricle (Figure 1.3).
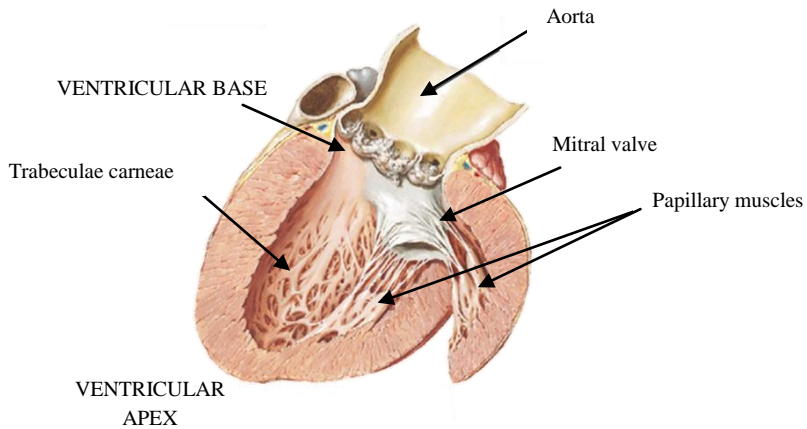
_____

Figure 1.3. Representation of a longitudinal section of a human left ventricle [2].

Depending on their morphology, three different types of ventricular trabeculae have been classified [4]:

- the "first type trabeculae", or papillary muscles, are anchored at one end to the heart wall and protrude towards the ventricular cavity. The chordae tendineae, which connect the papillary muscles to the mitral and tricuspid valve, are inserted at the top of these structures (Figure 1.3).
- the "second type trabeculae" are connected to the ventricular wall only at the terminal ends, in a bridge-like configuration;
- the "third type trabeculae" are anchored longitudinally along the muscular wall.

The papillary muscles have a specific function in heart mechanics: during ventricular contraction these muscles tighten the chordae tendineae and contribute to the coaptation of the atrio-ventricular valves leaflets; for this reason, they are often not considered as trabeculae, even if their morphology justifies the classification described above. This thesis focuses on the second and third type trabeculae, thus from now on the term "trabeculae" will be referred only to these two types of trabecular structures.

Due to their particular architecture, the trabeculae carneae give to the endocardial surface of ventricles a characteristic "spongy" aspect, in fact dividing the ventricular wall into two different layers: a trabeculated layer and a compact layer. During the diastole, the small invaginations formed by the trabecular network are filled by

_____

blood, which is expelled during the systolic phase of the cardiac cycle. The spongy structure of the trabeculated layer cannot be found in any other component of the circulatory system. Indeed, the luminal layer of blood vessels is extremely smooth in order to avoid blood stagnation and coagulation, typically promoted by irregular surfaces.

From a microstructural point of view the trabeculae are roughly homologous with the ventricular wall. The myocardium is composed for about the 70% of its volume by parallel cardiac muscle cells, or myocytes, having a diameter which varies between 10 and 20 µm and a length that ranges between 80 and 100 µm. The fundamental contractile unit in the cardiomyocytes is the sarcomere, which is about 2 µm long. The myocytes are composed by a series of 40-50 sarcomeres, and are connected one to each other by junctions optimized for the electrical stimuli conduction (intercalated disks). The cardiomyocytes are embedded in an extracellular matrix network, which represents the remaining 30% of cardiac muscle volume, where the collagen molecules (2%-5% of the interstitial components) form an organized structure connecting laterally the muscle fibres [5–8].

The only documented difference between the compact and the trabeculated myocardium composition regards the vascularization, which is lower in the trabeculae. Probably, the direct contact of trabecular myocytes with the blood in the ventricular cavity allows a higher mass exchange by diffusion; consequently, the trabecular myocytes are characterized by a lower capillary-to-myocytes ratio [3].

In the ventricular compact wall, the result of this hierarchical tissue organization is a complex three-dimensional muscular fibre architecture. The characteristic myocytes arrangement has been known by scientists since the XVI century and represents a key feature of heart behaviour. In particular, the cardiac fibres organization is the result of two contributes: a local and a global anisotropy.

The first contribute refers to a variation of the myocytes orientation through the heart wall thickness. Indeed, the cardiomyocytes are connected such that at any point in the normal heart wall there is a predominant fibres axis direction that is approximately tangent to the wall (within 3° to 5° in most regions [9]). This fibre axis rotates across the wall thickness, with a smooth transmural transition; thus, the ventricular wall can be seen as a composite of adjacent layers with the main fibres direction changing across the muscular thickness. In the left ventricle, the fibre angle varies from epicardium, where the mean angle is about -80° with respect to the circumferential direction, to the endocardium, where the cardiac fibres are oriented at about +80° [6, 10, 11] (Figure 1.4); therefore, the myocytes follow a left-handed helix at the epicardium, are preferentially arranged along the circumferential axis at

_____

the midwall and establish a right-handed helix at the endocardium. This particular architecture is the source of the heart local anisotropy.
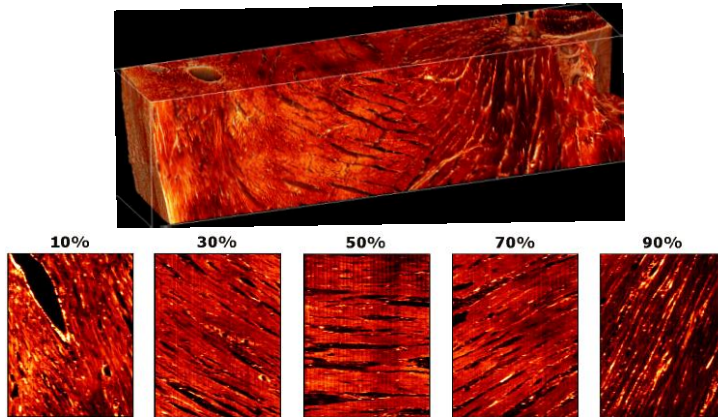

Figure 1.4. Upper figure: reconstruction of a transmural section of the ventricular wall. Lower figure: five section planes sliced at regular intervals from 10% (epicardium) to 90% (endocardium) of the wall thickness. Each plane is parallel to the epicardium [11].

The second contribution to the myocytes organization relates to a global anisotropy. Several studies have revealed a secondary structure of the myocardium, which can be seen as a unique band of muscle extending from the root of the pulmonary artery to the root of the aorta. This muscle bundle twists in two loops (apical and basal), resulting in the helical pattern which defines the two ventricular cavities (Figure 1.5) [12–14].

Figure 1.5. Structure of the ventricular muscular band. The band turns and twists to generate the two ventricular cavities [15].

19

_____

Focusing on the trabeculated layer, it is important to point out that the myocyte arrangement doesn't follow the spiral orientation just described for the compact myocardium; indeed, in the trabeculae, the cardiac fibres are parallel to the trabecular axis direction. This feature, together with the implicit assumption that the trabecular muscular tissue is homologous with the bulk myocardium, is one of the main reasons why the trabeculae are much favoured by experimentalists for the study of the ionic, mechanical, and metabolic function of the heart muscle.

Despite this wide use of ventricular trabeculae as experimental model for the characterization of the myocardial tissue, specific and quantitative information about the trabeculated layer are almost missing. Recently, some works have been developed in the literature in this field, mainly referred to a particular pathology called left ventricular non-compaction (LVNC). The LVNC is a primary cardiomyopathy of genetic origin which consists in an increase of the trabeculated layer thickness that can lead to heart failure, trombo-embolism and arrhythmia. The main criterion for the diagnosis of LVNC is the evaluation of the trabeculated mass with respect to the total ventricular mass by means of diagnostic imaging techniques (e.g. echocardiography and cardiac magnetic resonance). The physiologic amount of trabeculated mass in the left ventricle appears to be between the 12 and 17% of the total ventricular mass while, although this is not a universally accepted criterion, a trabeculated mass higher than about 20% of the ventricular mass is considered an index of pathology. The papillary muscles are usually excluded from this evaluation because of their specific role in heart behaviour, as mentioned above [16–19].

Hence, in the adult normal heart the second and third type trabeculae represent a significant percentage of the myocardial muscle mass, and not a mere geometrical peculiarity.

_____

1.2. EMBRYONIC TRABECULATION

The emergence of cardiac trabeculae in the ventricular lumen occurs during the embryonic development of the heart. In the embryonic stage the human heart evolves from a single peristaltic tube into an optimized four-chambered pulsatile pump. The level of organization in the heart structure increases with myocardium performances. The cardiac development involves different processes: growth, namely the change in myocardial mass, remodelling, the change in properties, and morphogenesis, the change in shape. During gestation the heart passes through several stages [20]. In the first days post-fertilization the myocardium, which is the first operating organ in the embryo, is a tube able to contract and generate a peristaltic wave. Initially, the tube collapses to avoid blood backflow, but soon after regional wall thickening, called endocardial cushions, start to behave as primitive valves, and the unidirectional flow is guaranteed even without a complete closure of the cardiac tube lumen. The next event in the heart development is cardiac looping: the myocardial tube bends and twists, laying out in the fundamental pattern of the four-chambered heart. During the looping process, the ventricular wall is thin, and the myocytes metabolic needs are supplied completely by diffusion from the heart lumen. At the same time with the subsequent wall thickening, one critical phase in the cardiac chamber maturation is the emergence of trabeculation in the luminal layers of the myocardium. At this stage the heart wall is composed primarily by a muscular trabeculae network surrounded by a thin epicardial compact layer (Figure 1.6).
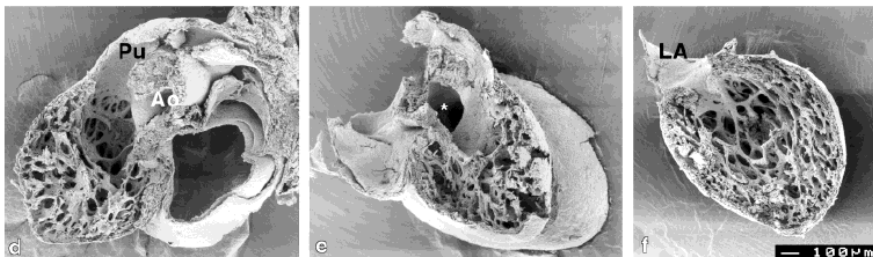

Figure 1.6. Sagittal dissections of a 41-days human embryo [20]. LA = Left Atrium, Ao = Aorta, Pu = Pulmonary artery.

_____

The trabeculated layer architecture is similar to the spongy bone, but growth and remodelling of muscle and bone tissues are different: whereas bone changes its morphology by material absorption and deposition due to external and internal forces, the myocardium variations in mass and orientation of cardiac fibres are achieved by cellular mechanisms like hyperplasia, hypertrophy and locomotion [21]. From a biomechanical point of view the myocardial trabeculation in the embryo has two major consequences: first, the trabeculae alter the stress distribution in the muscular wall; second, the blood flows through the inter-trabecular spaces, fulfilling the metabolic needs of the cardiac cells due to the increased surface area of the trabeculated myocardium. Therefore, the trabeculated architecture allows the myocardial mass to grow in the absence of a developed coronary circulation. Moreover, the shear stresses generated by intramyocardial blood flow might influence growth and morphogenesis, and the trabeculated pattern can also play a role in coordinating the electrical stimuli conduction.

After the completion of ventricular septation, further muscular mass increase results in a re-organization of the trabecular network architecture, which tends to orient in the apico-basal direction. Then, together with an increased body metabolic demand and the maturation of coronary circulation, the trabeculae start to coalesce, becoming the compact myocardium. This compact layer continues to modify and remodel until the maturation and organization of the adult myocardium is reached. As mentioned above, the percentage of the remaining trabeculated layer in the human adult heart is about the 12-17% of the total ventricular mass. This percentage depends on the species under consideration (for example in the lower vertebrates the heart is in general heavily trabeculated, while in birds the amount of compact myocardium is higher and the trabeculae are coarse with respect to the human heart) but a trabeculated layer is always present in adult animals [20], suggesting a role for this structural peculiarity in the behaviour of the physiologic heart.

_____

1.3. THE ROLE OF CARDIAC TRABECULAE: STATE OF THE ART

In the previous paragraphs the structure and the embryonic genesis of cardiac trabeculae were described. The main emerging points are that the trabeculae carneae represent a significant amount of the ventricular mass, which after the compaction of embryonic trabeculation remains and remodels in a specific pattern; moreover, an incorrect balance between the compact and the spongy myocardium seems to lead to cardiac pathology. These indications strongly suggest an influence of the ventricular trabeculae on heart mechanics. In spite of this evidence, the literature lacks of quantitative information about the trabecular network architecture and, consequently, the hypotheses about their possible functions are mainly just speculations.

During the last decades it was supposed that the arrangement and the microstructural composition of trabeculated layer could potentially influence different aspects of ventricular behaviour:

- ventricular fluid-dynamics;
- electrical stimulus conduction;
- ventricular mechanics;
- heart energetics.

In 1975, Burch hypothesised that the trabecular structure could contribute to the loss of kinetic energy of blood during diastole. Namely, the irregular trabecular surface would decrease the work necessary to stop the blood flow entering the ventricles, due to the increased area of the endocardial surfaces. Thus, the contraction force of heart muscle would only be used to eject blood from the ventricular cavities and no energy would be spent to reverse the fluid flow direction [22]. In another work, Burch also highlighted that in a smooth heart the circumferential shortening of the outer and inner ventricular walls might cause the endocardial surface to wrinkle, inducing possible injuries to the heart wall; conversely, an irregular internal surface like the trabeculated should reduce the wrinkling of the sub-endocardial layer during systole [23].

Otherwise, according to different theories, the cardiac trabeculae should reduce the flow turbulence during the systolic phase [24], or could have a function similar to the papillary muscles: during the ejecting period, the contraction of these finger-like structures could help the closure of the atrio-ventricular valves [25].

_____

All these assumptions are mainly based on empirical observations, and are not supported by quantitative data; one of the main reason is that an adequate identification of the trabecular network by diagnostic imaging, which is the primary method to analyse and reconstruct the cardiac geometry, is difficult because of the geometrical complexity of the trabeculated layer.

Only very recently in two different papers, Captur et al. [26] and Moore at al. [27] have characterized the internal ventricular surfaces using the fractal analysis. Both studies were aimed at evaluating the changing in fractal dimension of the endocardial border. In particular, it was found that this dimension varies during the cardiac cycle, with an increase during diastole and a subsequent decrease during systole. Since the fractal dimension depends on the size of the inter-trabecular spaces, a variation in this index is a first quantification of the geometrical changes that the trabeculated layer undergoes during the heart cycle.

Accordingly, the fluid-dynamic modelling of the interaction between the blood and the trabeculated surface of the left ventricle has lately shown that the fluid "entrapped" into the trabeculated layer during diastole is expelled by heart contraction, helped by trabecular activity that tends to close the inter-trabecular spaces. This contribution is more evident in case of cardiac pathologies which affect the ventricular wall kinematics: in the presence of these pathologies the trabecular contraction is not efficient, and the blood stagnates for a longer period in the spaces between trabeculae, increasing the risk of coagulation [28].

Moreover, Bishop and Planck have recently developed an anatomically detailed biventricular computational model of a rabbit heart to understand if the trabeculae and the papillary muscles could interact with excitation wavefronts during cardiac arrhythmias [29, 30] (Figure 1.7). The comparison between the complex model with respect to a simpler model (i.e. a model with no fine-scale geometrical structures) showed that the overall dynamics of tachyarrhythmias is very similar in the two cases examined: the inclusion of the trabeculated layer didn't affect significantly the model outcomes.
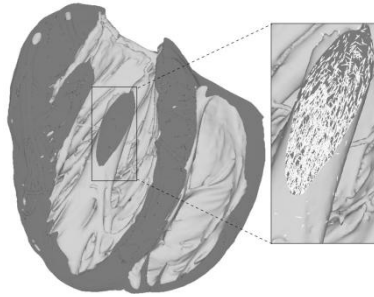
_____

Figure 1.7 Geometry and a detail of the vector fibres orientation in the papillary muscle of the rabbit model of Bishop [30].

The results described above are extremely partial and do not allow a satisfactory understanding of the role of the trabeculae on the ventricular performances. A complete study should take into account electro-mechanics, fluid-dynamics and energetics of the ventricles. Nevertheless, the primary heart function of pumping blood is fundamentally mechanical, hence the study of the mechanical role of the trabeculae seems to be the foundation of any further investigation.

_____

Chapter 2 :

AIMS

_____

2.1. MOTIVATIONS

The heart is an essential organ for maintaining human life by providing the blood with the necessary energy to flow throughout the circulatory system. The study of heart behaviour is a challenging research field since it requires the understanding of several mechanisms, i.e., electrophysiology, fluid-dynamics, mechanics and energetics. The description of each of the events occurring during the heart cycle involves the complex interaction of all these disciplines, both at a microscopic and a macroscopic level. In this framework, computational modelling has acquired more and more relevance, thanks to a dramatic increase in the computational resources and methods. As a consequence, many simulation studies have been reported in the literature so far, characterized by a growing integration of different physical phenomena [31–34].

Within this encouraging context, several aspects of cardiac behaviour are still unclear, and among these the presence of cardiac trabeculae on the ventricular wall is almost disregarded. In the previous chapter, an overview of the state of the art about the influence of the cardiac trabeculae on heart behaviour was made. What clearly comes to light is that, despite the evidences of a significant contribution of cardiac trabeculae on the physiologic behaviour of the ventricles, the research about this peculiarity of the heart structure is surprisingly missing up to now.

At present, the remarkable improvement in medical imaging techniques allows the reconstruction of patient-specific cardiac geometries which can be integrated in computational models to study the influence of specific shape features on heart performance [35–37]. Nevertheless, the geometrical models are usually limited to the gross heart anatomy: the trabecular network complexity have deterred a deep investigation of the architecture and characteristics of the trabeculated layer. Consequently, the role of ventricular trabeculae on heart behaviour is basically still unknown, as well as the implications of a change in the physiologic trabeculated layer structure.

The aim of the project was the development of a tool suitable to study the influence of the trabeculae carneae on ventricular performances. As previously highlighted, a complete analysis should take into account all the different physics involved in heart functioning, because the trabeculated layer can play a role in each one of these mechanisms. Even so, the main goal of the thesis was the investigation of the role of the cardiac trabeculae exclusively on ventricular mechanics, since the heart is primarily a pump. The investigation of a possible biomechanical role of trabeculae

wants to lay the foundations for further studies which will be needed to deepen the understanding of the influence of trabeculae on heart functions.

2.2 AIMS

In this project a computational model aimed at studying the influence of the cardiac trabeculae on ventricular mechanics was developed. The specific work target was the comparison between the behaviour of a trabeculated and a "smooth" ventricle, to understand the differences induced by the presence of the spongy myocardium on ventricular performances. A computational approach was adopted in order to perform a parametric study setting specific model features, like the ventricular muscular mass and the intra-ventricular cavity volume, for an adequate comparison within different models. In summary the main objectives of the Ph.D. thesis were:

- to develop two ventricular geometries: a trabeculated model and a smooth model of the left ventricle, having the same wall muscular mass and an equal inter-ventricular cavity volume;

- to describe a physiologic cardiac fibres distribution for both the smooth and the trabeculated model;

- to identify a suitable constitutive relationship for the cardiac tissue and to optimise the material parameters; the material modelling includes both the passive and the active myocytes behaviour;

- to define adequate boundary conditions, which comprises the implementation of a preload and an afterload circuit simulating the systemic circulation;

- to simulate the entire heart cycle for both the trabeculated and the smooth model;

- to study the effects induced by the variation of some parameters of interest of the trabeculated layer (e.g. trabecular mass, size etc.).

According to these main objectives, the thesis organization is described hereinafter. In **Chapter 3** the implementation of the finite element model is explained. In particular, the ventricular geometries are described in section 3.1, while the ventricular wall modelling (constitutive relationship and myocytes architecture) is

_____

presented in section 3.2. In the next sections the boundary conditions and the other simulation conditions are described.

The results of the computational simulations are shown in **Chapter 4**. These results include the comparison between the trabeculated and the smooth model outcomes (section 4.2), the evaluation of the influence of the trabeculated layer parameters (section 4.3) and the implication of the presence of the ventricular trabeculae on heart physiology (section 4.4). Finally, in **Chapter 5** the results of the study are discussed and the conclusions are pointed out.

_____

Chapter 3 :

COMPUTATIONAL MODEL
OF THE LEFT VENTRICLE

To understand the influence of the cardiac trabeculae on heart performances a finite element model of the left trabeculated ventricle was implemented. The results obtained with this model were compared with the outcomes of a smooth ventricular model having the same muscular mass and intra-ventricular volume. In this chapter the implementation of these models will be described.

_____

During the last two decades numerical and computational techniques have assumed a central role in the interpretation, understanding and simulation of physiological functions of whole organ systems. This has been possible thanks to the improvement of computational algorithms and parallel increase in availability of high performance computing resources, as well as to the collection of new experimental data at the cell, tissue and organ levels. The study of heart behaviour is one of the field in which computational modelling can provide greater insight about the organ physiology and patho-physiology. The anisotropy and non linear behaviour of the cardiac tissue, as well as the large deformations involved in the heart cycle simulation, are the main reasons that make the computational approach much favoured with respect to the analytical approach. Besides, due to the high ventricular wall-thickness-to-radius ratio, even the most sophisticated thick-walled shell theories are inadequate to mathematically model the ventricular mechanics [38]. Conversely, numerical modelling allows a better understanding of the complex mechanisms at the base of cardiac behaviour and can guide the design of new successful treatment strategies.

In the development of a computational model of ventricular mechanics the main issues to be considered are: an adequate description of the three-dimensional geometry and of the structure of the myocardium; the identification of a realistic constitutive equation, together with a suitable parameters estimation; the formulation of balance laws and boundary conditions for the solution of the continuum problem. In the literature, several models have been implemented so far for a deeper understanding of the ventricular mechanics. Some of these models are based on biventricular geometries and patient-specific material optimization [35], multi-scale approaches [33, 39, 40] and fluid-structure interaction to simulate the blood flow into the ventricle [41].

Despite this, none of these models accounts for the presence of the cardiac trabeculae at the endocardium. In this work, a finite element model of the left ventricle specifically designed to study the influence of the trabeculated layer on ventricular mechanics was developed. The finite element problem was solved by means of the commercial code Abaqus (Abaqus® 6.10, SIMULIA, Dessault Systémes.).

_____

3.1. VENTRICULAR GEOMETRY

From a mechanical point of view, the ventricles are basically thick-walled pressure vessels, which substantially vary wall thickness and curvature during the cardiac cycle. The ventricles are the most important chambers in the heart since they pump the blood in the cardiovascular system; on the contrary, the atria are mainly thin-walled reservoirs at low pressures, not having a prominent mechanical role. The right and left ventricles have similar weights at birth, but in an adult individual the left ventricle represents the major part of the myocardial mass: in fact the left ventricle provides the distribution of blood into the systemic circulation, which is characterised by an higher hydraulic resistance with respect to the pulmonary circulation; thus, the left ventricle works at higher pressure than the right ventricle. To support this higher pressure, the left ventricle needs a thicker muscular wall and, consequently, a greater muscular mass. Therefore, in this work only the left ventricle was modelled.

In order to reveal possible differences in ventricular mechanics due to the spongy myocardial layer existence, the basic idea was to compare two different models: a trabeculated model and a smooth model, namely one model with and one without the trabecular layer. To permit an appropriate comparison between the two cases, some geometrical parameters were set in the ventricular initial configuration. In particular:

- the ventricular total mass: the mass of muscle must be equal for both models as the amount of muscular tissue can affect the ventricular behaviour in both the systolic and diastolic phase;

- the ventricular cavity volume: for a correct evaluation of ventricular volume changes, the intra-ventricular volume was set in the initial configuration.

In order to meet these specification, and to find a good compromise between an accurate geometrical description and computational costs, the left ventricle was modelled by an ellipsoidal shape. Actually, the left ventricle anatomy is characterized by a spatially variable thickness and curvature; the ventricular wall is thickest near the cardiac base and equator and thinnest near the apex. However, the gross anatomy of the left ventricle can be well approximated by a thick-walled ellipsoid of revolution truncated at the base level (Figure 3.1), as suggested by previous works [42–46]. Thus, this simplified geometry was chosen in both the smooth and the trabeculated case. The main difference between the two models

_____

shape is the endocardium morphology: while the inner ventricular surface is represented by a regular ellipsoid in the smooth configuration, in the trabeculated model the trabeculae carneae are attached to the endocardial surface. Thus, while the wall thickness is constant in the smooth geometry, it varies spatially in the presence of the trabeculae.

The geometrical models were designed by means of the CAD software Rhinoceros® 4.0 (McNeel, Seattle, WA, USA). The detailed description of the smooth and the trabeculated geometries, as well as the models discretization necessary for the finite element formulation, are presented in the following sections.

3.1.1. Smooth model

The ventricular cavity of the smooth model was represented by an axisymmetric ellipsoidal shape truncated at about 2/3 of the long axis.

To define the ventricular initial configuration, attention should be paid in the definition of the reference stress free state. Firstly, residual stresses are present in the ventricular wall at zero pressure; these stresses are the result of the cardiac growing and remodelling processes, and can affect the wall stress and strains [47]. However, the experimental evaluation of these residual stresses is not straightforward, and quantitative data are difficult to be found. Thus, an initial stress free configuration was considered and the residual wall stresses disregarded.

Secondly, the zero-pressure configuration should be defined. Indeed, at the beginning of the first simulated cycle the ventricle is characterized by an internal pressure of 0 mmHg, while the end-systolic pressure is higher than zero. Hence, a reference ventricular volume at zero-pressure lower than the end-systolic volume (ESV) was considered. In particular, the ellipsoid describing the smooth endocardial surface is characterized by a minor semi-axis of 14 mm and a major semi-axis of 57 mm, according to previous works [48–50]. Consequently, the ventricular cavity volume was set at 43 ml in the initial, stress free configuration. A constant wall thickness of 9 mm was considered, thus obtaining epicardial minor and major axes of 23 and 66 mm respectively and a ventricular wall volume of about 93 cm^3. The resulting geometrical model is shown in Figure 3.1.
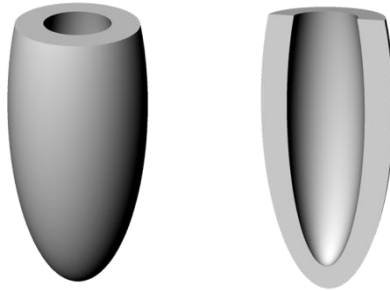
Figure 3.1. Geometry of the smooth ventricular model. Left: exterior view. Right: axial section.

3.1.2. Trabeculated model

The cardiac trabeculae anatomy and structure was discussed in Chapter 1. The complexity and irregularity of the trabeculated layer architecture make it difficult the realistic reconstruction of the endocardial surface from e.g. diagnostic images. Furthermore, a patient-specific geometry doesn't allow neither a parametric investigation of the spongy myocardium structure nor a comparison with the smooth ventricular model at the same ventricular mass and intra-ventricular volume. For these reasons, the left trabeculated ventricle was basically represented like the smooth model by an axisymmetric ellipsoidal shape having the same epicardial minor and major semi-axes (23 mm and 66 mm respectively). To design the trabeculated pattern keeping constant the intra-ventricular volume and the muscular mass, a set percentage of the total muscular mass was changed from compact layer to trabeculae at the endocardium. This variation in the inner surface configuration induces a thickness decrease in the inter-trabecular spaces and a thickness increase at the trabeculae. Since the trabeculae are preferentially oriented along the apico-basal direction in the physiologic case, they were described as cylindrical strands oriented along the ventricular axis direction, laying onto the endocardium. Hence, the ventricular trabeculated geometry was simplified in order to allow a parametric study to be performed (e.g. changing the trabecular diameter), obtaining more general results without losing the main features of the structure.

In particular, to optimize several aspects of the ventricular model (i.e. the material parameters, section 3.2.3; the pre and afterload circuit components, section 3.4.1), a reference trabeculated model was implemented. This model was characterized by a trabecular mass equal to the 15% of the total muscular mass (about 14 cm^3);

moreover, the trabeculae were oriented in the apico-basal direction and were characterised by a diameter equal to 4 mm (Figure 3.2). This model was considered as the model of reference for the comparison with the smooth model, since all the parameters of the trabeculated layers were set at the physiologic mean value.
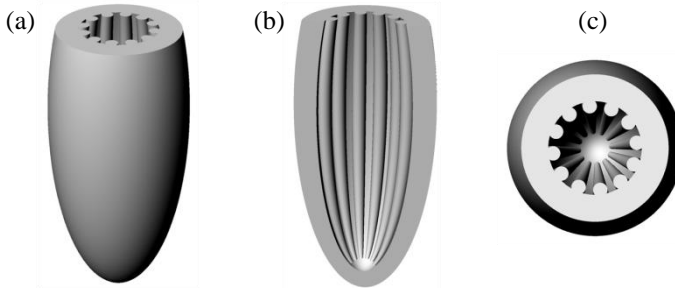

Figure 3.2. Trabeculated ventricular model: (a) exterior view, (b) axial section, (c) top view.

Different trabeculated models were implemented to further investigate the influence of some geometrical parameters of interest on the model outcomes. In particular, these parameters were:

- the trabecular mass;
- the trabeculae dimension;
- the orientation of trabeculae at the endocardium.

Trabecular mass

As highlighted in section 1.1, the physiologic trabecular mass varies between the 12% and the 17% of the total ventricular mass in a healthy subject, while a trabecular mass higher of the 20% is usually considered an index of pathology. To investigate the possible influence of the trabeculated layer mass percentage on ventricular behaviour, two different trabeculated mass were considered in addition to the reference one (15%), in particular the 7% and the 22% of the ventricular mass (Figure 3.3).
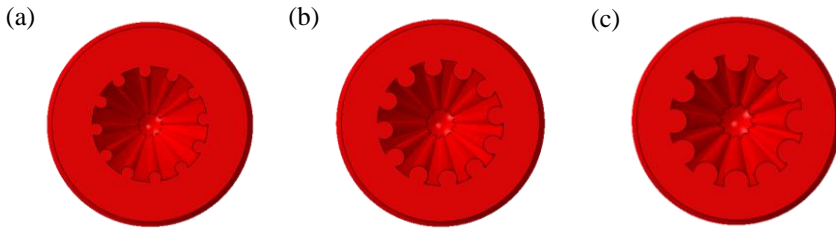
(a)   (b)   (c)

Figure 3.3. Top view of the trabeculated models with a trabecular mass of (a) 7%, (b) 15% and (c) 22% of the total ventricular mass.

This variation in trabecular mass means a change in the compact wall thickness: the higher the trabeculated layer mass, the thinner the compact layer depth. Table 3.1 summarises the maximum and minimum wall thickness for all the models.

Table 3.1. Maximum (t_{max}) and minimum (t_{min}) wall thickness for the smooth and the trabeculated models with different spongy layer mass.

	Smooth	7%	15%	22%
t_{min} [mm]	9	8.2	7.25	6.5
t_{max} [mm]	9	10.3	10.45	10.1
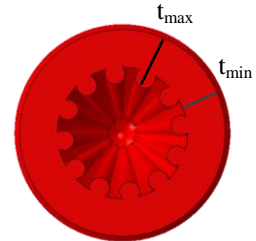
Trabeculae dimension

The cardiac trabeculae size is variable in the physiologic left ventricle, but no specific experimental data are available about their dimensional range. Generally speaking, in echocardiografic analyses the myocardial trabeculations are identified as localised protrusions of the endocardial surface with a diameter higher than 3 mm [18, 51]. To study the influence of the trabecular size only, three different diameters of the trabeculae were adopted at a constant spongy layer mass percentage of 15%: 5.2 mm, 4 mm and 3.4 mm (Figure 3.4). The compact layer thickness is the same for all the models (7.25 mm, see Table 3.1), while the maximum wall thickness decreases if the trabeculae diameter is reduced (Table 3.2). Within each model, all the trabeculae have the same diameter.

_____

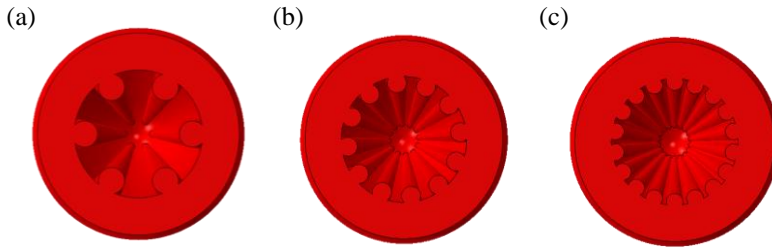(a)   (b)   (c)

Figure 3.4. Top view of the trabeculated models with different diameters of the trabeculae. The trabecular diameter is equal to (a) 5.2 mm, (b) 4 mm and (c) 3.4 mm.

Table 3.2. Maximum wall thickness (t_{max}) of the trabeculated models characterized by different trabeculae diameter and a trabecular layer mass equal to the 15% of the total mass.

Trabeculae diameter [mm]	5.2	4	3.4
t_{max} [mm]	11.85	10.45	9.6

Trabeculae orientation

Even if the preferential direction of the cardiac trabeculae is along the ventricular axial direction, the myocytes orientation at the endocardium, as well as the heart macrostructure which is the result of the twist of the muscular band (section 1.1), suggest an inclination of the ventricular trabeculae with respect to the circumferential direction. For this reason another trabeculated model was developed to analyse a possible influence of the orientation of the trabeculae. This model is characterized by an inclination of the trabecular pattern of about 60° at the mid-axis level with respect to the circumferential direction (Figure 3.5). The choice of this angular value was indicated by literature works about the cardiac fibres architecture [10], and by observations on the reconstruction of the ventricular cavity obtained by laser technique (see Appendix A). The mass of the spongy layer was set at the physiologic value (15% of the total muscular mass), while the trabeculae have a diameter of 4 mm.

_____

(a)   (b)   (c)
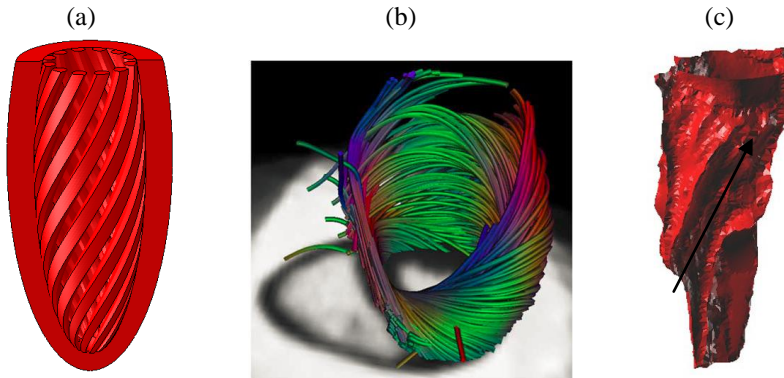

Figure 3.5. (a) Trabeculated model with an inclination of trabeculae of 60° with respect to the circumferential direction (part of the compact layer was removed for a better view of the trabeculated pattern); (b) fibres orientation in the left ventricle and short axis MRI slice (the colouring depends on the fibres orientation) ([52] ,Copyright © 2012, IEEE); (c) laser reconstruction of the ventricular cavity (see Appendix A). The arrow indicates the trabecular direction

3.1.3. Discretization

To perform the finite element analyses all the models were discretized. The geometry discretization is crucial in the implementation of a computational model, because from this process depend both the convergence and the accuracy of the solution. Of course, an increased number of elements implies an higher accuracy of the solution, but higher computational costs too. Thus, the number of element is always a compromise between this two objectives: precision of the solution and computational time. In this work, all the models were discretized with 8-node hexahedral elements by using the software Ansys Meshing® (ANSYS Inc., Canonsburg, PA, USA). Linear interpolation functions were chosen since the presence of fluid elements to model the ventricular cavity (section 3.3) didn't allow the use of higher order shape functions. The number of elements for each model was chosen also considering the fibres orientation in the ventricular wall; indeed, the ventricle is composed by discrete sheets of parallel myocytes, with a changing fibres orientation in the wall thickness (section 1.1). Thus, in the compact myocardium an adequate numbers of "sheets", namely the number of elements along the wall thickness, were set to obtain a smooth variation in the myocytes orientation. The number of sheet was kept as constant as possible among all the models to avoid any

_____

difference in the fibres orientation of the compact layer. In particular, the number of sheet is equal to 9 for all the models with the exception of one trabeculated model, for which a higher number of layers was required. Hence, a number of elements equal to 18 along the wall thickness was set in this case, such that setting the same fibre orientation for two sheets in a row the standard number of nine different myocytes orientation in the ventricular wall was obtained. In Figure 3.6 the mesh of the smooth model, of one trabeculated model and of the model with oblique trabeculae are shown. A different number of elements was required for each model; a higher number of elements was always necessary for the trabeculated models with respect to the smooth case due to the geometry complexity. In Table 3.1 the number of elements of all the models is summarized.

(a)

(b)
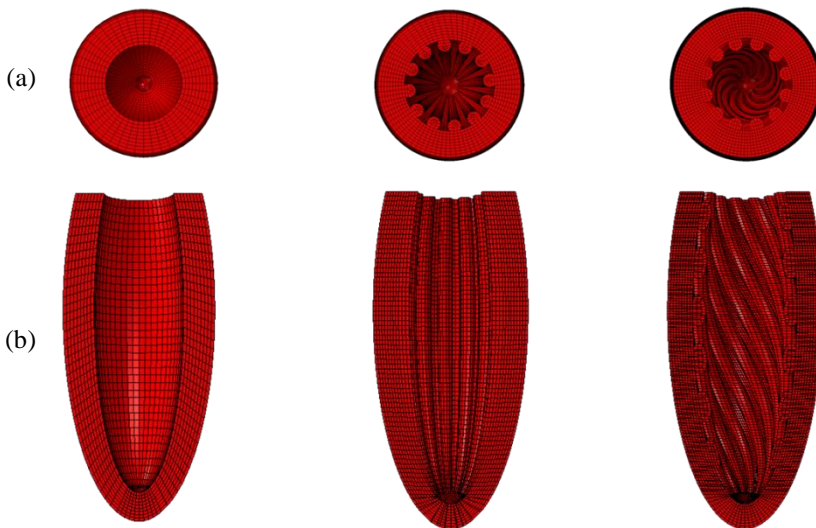
Figure 3.6. Top (a) and axial sections (b) of three discretized ventricular models: the smooth model (left), the reference trabeculated model with longitudinal trabeculation (centre) and the model with oblique trabeculae (right).

_____

Table 3.3. Number of elements of all the implemented models. The mass percentage represents the mass of the trabeculated layer with respect to the total ventricular mass, while d_t is the cardiac trabeculae diameter.

Model	Smooth	Trabeculated					
		Axial trabeculae					Oblique trabeculae
		Mass 7%	Mass 15%			Mass 22%	Mass 15%
		d_t 10.3mm	d_t 3.4mm	d_t 4mm	d_t 5.2mm	d_t 10.1mm	d_t 4mm
Number of elements	17730	81915	144342	60921	357503	159858	147651

_____

3.2. VENTRICULAR WALL MODELLING

In the mechanical modelling of the cardiac wall, two major features should be considered for a realistic model response: the peculiar myocytes arrangement in the ventricular wall and the constitutive relationship for the simulation of the myocardium mechanical behaviour, which should be defined in an appropriate theoretical framework for the description of the material stress and strain.

3.2.1. Wall fibres architecture

The cardiac fibres architecture was described in section 1.1. The ventricle is characterized by a complex three-dimensional structure of the myocytes which influences various heart functions, including the electrical stimulus conduction and the ventricular mechanics [53]. The fibrous nature of the heart has been known for centuries; in 1628 Harvey described in *De motu Cordis* the functional role of the cardiac fibres [54], but until the half of the XX century the descriptions were largely qualitative. After the works of Streeter [10], [46], the first extensive researches about the orientation of fibres in the canine left ventricle, many studies have been reported; at present, one of the most powerful method to assess the myocytes arrangement is the Diffusion Tensor MRI (DT-MRI), a technique that measures the self-diffusion of protons in fibrous tissues which allows the non-invasive visualisation and quantification of the myocytes direction in the cardiac wall [52, 55, 56]. What clearly emerged from these studies is that the ventricular wall is composed of discrete layers (or sheets) of aligned cardiac fibres, which are the predominant fibre types (~70% of the muscle volume), tightly bound by collagen endomysial fibres; the perimisial collagen couples the different sheets but allows an easy sliding of the muscular layers over each other [11, 57]. The orientation of the muscular sheets changes along the wall thickness, describing a characteristic helical pattern. In particular, the myocytes orientation is equal to about -80° with respect to the circumferential direction at the epicardium and reaches about +80° at the endocardium, with an almost linear variation along the wall thickness [10]. A recent statistical analyses on the fibres architecture variation in a population of human hearts has revealed that the fibres orientation is quite preserved between individuals [52]. The heart muscle layered organization can be described by an orthonormal set of basis vector which characterize the fibres orientation at each point of ventricular wall; the first axis $\mathbf{f_0}$ is referred to the cardiac fibres direction, the second axis $\mathbf{s_0}$ lies

_____

in the myocytes sheet plane and is perpendicular to the fibres direction (cross-fibres axis), and the third axis $\mathbf{n_0}$ is normal to the sheet plane (Figure 3.7).
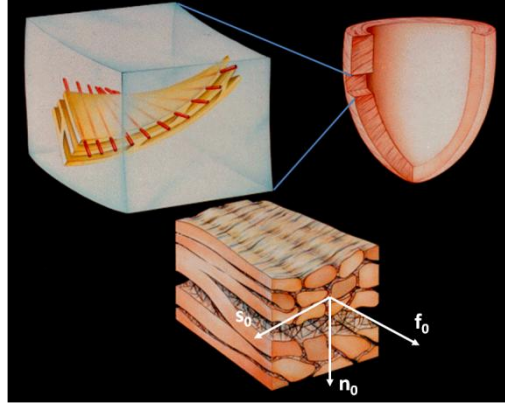

Figure 3.7. Schematic representation of the fibres arrangement in the left ventricle (top right) wall. The myocytes (top left, in red) orientation rotates along the wall thickness. At the bottom, the interconnection between the sheets is represented: the perymisial collagen connects the adjacent sheets, while the endomysial collagen bound the myocytes within the single sheet (adapted from [37]).

To replicate the physiologic fibres architecture in the ventricular models, a routine was implemented using MATLAB$^®$ (The MathWorks, Inc, Natick, MA, USA); the algorithm assigns at each element of the mesh the orthonormal basis which defines the myocytes orientation in the reference configuration. To do this, first the circumferential, radial and axial direction are identified for each element at the element centroid; then, the circumferential and longitudinal axes are rotated in the sheet plane to obtain the three axes $\mathbf{f_0}$, $\mathbf{s_0}$, $\mathbf{n_0}$. Since the myocytes orientation is almost constant along the circumferential and longitudinal direction [55, 56], a variable cardiac fibres angle was assigned only along the wall thickness in order to obtain the discrete layers arrangement. In Figure 3.8 the myocytes arrangement is shown for the different types of model. Note that, as highlighted in section 1.1, the myocytes in the trabeculae are oriented along the trabecular axis direction. Thus, the -80°/+80° transmural range was kept constant for the compact layer also in the trabeculated models, but an axial orientation was established for the trabecular structures. To ensure un equal number of sheets (namely, an equal number of different orientations across the wall) between all the models, the radial

_____

discretization was set by fixing the number of element across the ventricular wall (see section 3.1.3)
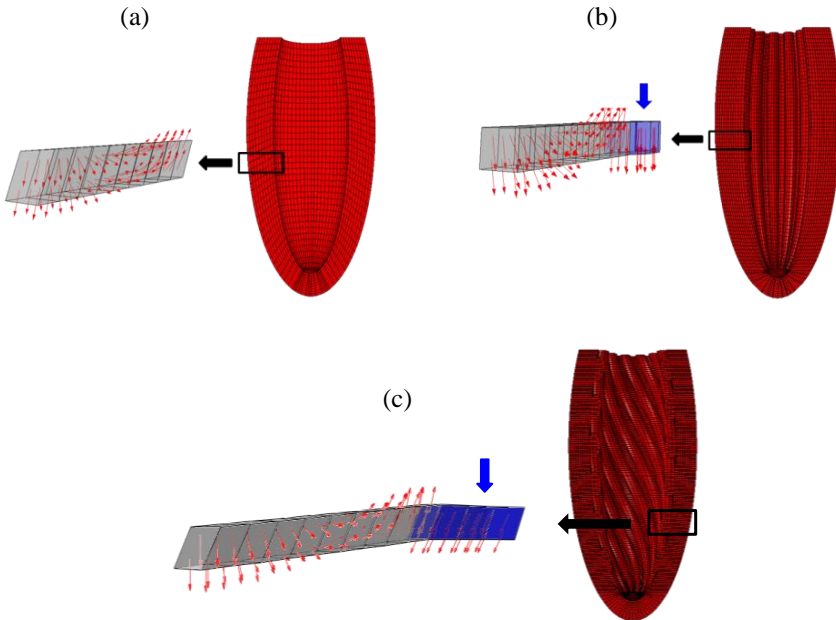

Figure 3.8. Fibres orientation in (a) the smooth model, (b) the reference trabeculated model and (c) the trabeculated model with oblique trabeculae. The trabeculated layer is coloured in blue, while the compact layer is grey.

3.2.2. Finite deformation elasticity

Kinematic relations

During the heart cycle, the cardiac tissue undergoes deformations which are higher than the 20%. When the material is subjected to such large displacements, the reference configuration is different from the actual configuration; thus, for the description of the kinematic relations, the finite deformation theory must be used, since the linearization introduced by the small deformation assumption would lead to inacceptable errors in the stresses and strains calculation.

Let the reference (undeformed) configuration of a generic body at the reference time $t_0 = 0$ be Ω_0, while Ω is the current configuration after the motion of the same

continuum. The vector $X = (X_1, X_2, X_3)$ defines the position of a point in the reference configuration; the same point in the actual configuration is characterized by the vector $x = (x_1, x_2, x_3)$. The point vectors in the reference and current configuration are referred to a common reference system, i.e. an orthonormal basis fixed for all the time t. The motion equation χ is the one-to-one relationship which maps all the material points from Ω_0 to Ω, such that $x = \chi(X, t) \; \forall \; x \in \Omega$. This relationship represents the continuous, differentiable, invertible trajectory of each material point. Is then possible to define the *deformation gradient F* as

$$F = \frac{\partial \chi(X, t)}{\partial X} = \frac{dx}{dX} \qquad .$$

(3.1)

The Jacobian of the transformation $J = det(F)$ (3.2) is known as the volume ratio, and it describes the volume body changes during the deformation process. Since F is invertible, $J \neq 0$; moreover, because of the impenetrability matter, negative volumes are rejected, thus $J > 0$ for all $X \in \Omega_0$ and for all the t. If $J = 1$, there are no volume changes between the reference and the current configuration, and the material is incompressible.

In general, F has nine components for each time t, and it defines how a line element in the undeformed configuration dX changes in the current configuration to the corresponding line element dx. The deformation gradient can be split into two contributes: a rotational component and a stretch component. Hence, it can be written that $F = RU$, where R is the orthogonal rotation tensor and U is the symmetric positive definite stretch tensor. It's important to highlight that U contains all the information about the body strains, without considering the rigid body motions. Conversely, F is in general non-symmetric and contains both the material strains and rigid rotations, so other quantities are usually defined to describe the body deformation. In particular, deriving the *right Cauchy-Green tensor* by $C = F^T F$, a symmetric and positive definite deformation tensor is obtained. Now the *Green-Lagrange strain tensor E* can be written as

$$E = \frac{1}{2}(F^T F - I) = \frac{1}{2}(C - I)$$

(3.3)

_____

where I is the second order identity tensor. Note that if $C = I$ the line element is unstretched and there is no relative motion of material points under χ. Consequently, the E vanishes and the body doesn't change in size and shape.

There are three invariants of C, namely three linear combination of the components of C, which don't change under coordinate rotation at a fixed state of deformation:

$$I_1 = tr C \qquad I_2 = \frac{1}{2}[I_1^2 - tr(C^2)] \qquad I_3 = \det C \quad .$$

(3.4)

These quantities are useful in the definition of the material constitutive law.

Stress measures

Consider the body at a certain time t under the action of internal and external forces on the volume V and on the body surface $\delta\Omega$; let the body be cut by a plane that passes through a generic point $x \in \Omega$.

The plane separates the body into two parts; focusing on one of these parts, the infinitesimal surface ds which surrounds the point x is characterized by a vector normal to the surface n. An infinitesimal actual force df acts on the surface ds; this force is the result of the interaction of the two portions across the plane surface. The quantities x, n and ds in the deformed, current configuration are indicated as X, N and dS in the reference, undeformed configuration. Thus, for every surface element, holds the relation

$$df = t ds = T dS$$

(3.5)

where

$$t = t(x, t, n) \qquad T = T(X, t, N) \quad .$$

(3.6)

In these equations, t represents the *Cauchy (or true) traction vector*, referred to the actual configuration, while T is the *first Piola-Kirchhoff traction vector*, described with respect to the reference configuration (Figure 3.9).
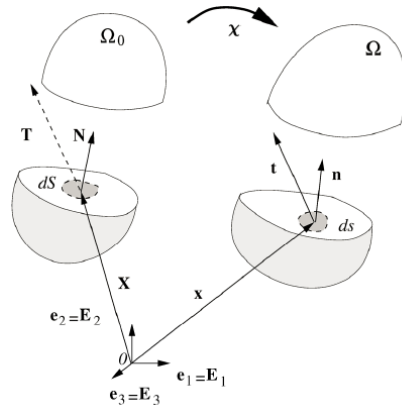
_____

Figure 3.9. Schematic representation of the traction vectors in the reference and actual configuration.

In addition, for the *Cauchy's stress theorem*, it is possible to write

$$t = t(x, t, n) = \sigma(x, t)n \qquad\qquad T = T(X, t, N) = P(X, t)$$

$$(3.7)$$

where σ is the symmetric tensor field called *Cauchy (or true) stress tensor* and P denotes the *first Piola-Kirchhoff (or nominal) stress tensor*, which is in general non symmetric. These two tensors are related by the transformation $P = J\sigma F^{-T}$, where J has been defined in Eq. (3.2); this relationship enables to switch from the true to the nominal stress tensor. Many other definitions of the stress tensor exist; two of the most used are the *Kirchhoff's tensor* τ, defined as $\tau = J\sigma$, and the *second Piola-Kirchhoff stress tensor* S, equal to $S = F^{-1}P$. The second Piola-Kirchoff stress tensor does not admit a physical interpretation, but is convenient because, instead of P, it is a symmetric tensor.

Hyperelasticity

The kinematic and stress relations just described, as well as the balance principles for the formulation of the continuum problem, are at the base of any mechanical problem and are valid for all types of materials. To solve a specific problem, the description of the peculiar material behaviour, namely the constitutive law, is needed. The *hyperelastic constitutive theory* is an ideal framework for the definition

_____

of the mechanical response of the cardiac tissue, even if, like all the constitutive relationships, it is an approximation of the real material behaviour under some conditions of interest. The definition of a hyperelastic material postulate the existence of a *Helmholtz free energy function* ψ defined for unit volume. If $\psi = \psi(\mathbf{F})$, than the Helmholtz energy is referred to as *strain energy function*; equivalently is possible to write the strain energy function considering the Cauchy-Green tensor as argument ($\psi = \psi(\mathbf{C})$). The hyperelastic materials set is a subclass of the elastic materials set for which the material stress can be calculated by deriving the strain energy with respect to the material deformation gradient

$$\mathbf{P} = \frac{\partial \psi(\mathbf{F})}{\partial \mathbf{F}}$$

(3.8)

or alternatively

$$\mathbf{S} = \frac{\partial \psi(\mathbf{E})}{\partial \mathbf{E}} = 2 \frac{\partial \psi(\mathbf{C})}{\partial \mathbf{C}} \quad .$$

(3.9)

Also, is possible to write the decoupled form of the strain energy function as

$$\psi = \psi_{vol}(J) + \psi_{dev}(\overline{\mathbf{C}})$$

(3.10)

where the first term relates to a volumetric part while the second term refers to a deviatoric (isochoric) part. $\overline{\mathbf{C}}$ is the *modified Cauchy-Green tensor*, which is equal to

$$\overline{\mathbf{C}} = J^{-2/3}\mathbf{C} \quad .$$

(3.11)

In addition, the deviatoric part of the strain energy can be further divided as

$$\psi_{dev} = \psi_{iso}(\overline{\mathbf{C}}) + \psi_{aniso}(\overline{\mathbf{C}})$$

(3.12)

in the sum of an isotropic and an anisotropic part. For incompressible materials, as mentioned above, $J = 1$; these materials are called constrained materials. A generic constitutive equations of an incompressible material has the form

_____

$$\psi = \psi(\boldsymbol{F}) - p(J - 1)$$

(3.13)

where p is an indeterminate Lagrange multiplier which can be defined as *hydrostatic pressure*. The calculation of p is possible only by means of the equilibrium equations and the boundary conditions.

Referring to Eq. (3.8) and (3.9), and known that $\boldsymbol{\sigma} = J^{-1}\boldsymbol{F}\boldsymbol{S}\boldsymbol{F}^T$, the Cauchy stress tensor for an hyperelastic incompressible material can be derived as

$$\boldsymbol{\sigma} = \boldsymbol{F}\frac{\partial \psi}{\partial \boldsymbol{F}} - p\boldsymbol{I} \ .$$

(3.14)

To characterize the material response, each one of the term which constitutes the strain energy function must be specialized for the peculiar material under examination. In the following section the specialisation of the strain energy for the cardiac tissue will be described.

For a complete treatment of the finite hyperelasticity theory see "Nonlinear solid mechanics" by Holzapfel [58].

3.2.3. Constitutive model for the cardiac tissue

The myocardium, like most of the biological tissues, exhibits an highly non-linear, anisotropic stress-strain behaviour. In particular, the stiffness of the material is higher in the cardiac fibres direction ($\mathbf{f_0}$, see Figure 3.7), with respect to the other two directions ($\mathbf{s_0}$ and $\mathbf{n_0}$) [59–61]. To model the mechanical response of the myocardium, several features of the cardiac muscle should be considered. First, the cardiac tissue is characterized by both a passive and an active behaviour; thus, to model the diastolic and the systolic phase of the heart cycle, both the passive tissue behaviour as well as its active contraction must be modelled by an adequate constitutive relationship. Second, the material parameters of the constitutive law must be identified to obtain a realistic material deformation against physiologic load conditions. Finally, the structure behaviour must be considered: the material optimization should lead to a realistic ventricular response in terms of pressure-volume relationship, as well as stress and strains in the cardiac wall.

In the literature several constitutive laws have been proposed for cardiac tissue modelling, starting from elastic, isotropic laws in the first models of the ventricle

_____

[62] to orthotropic relationships in the most recent works [37, 63, 64]. Despite this, a full characterization of this biologic material has not been reached yet. The available experimental data usually come from standard mechanical tests (uniaxial [61], bi-axial [59] or shear tests [60]), which do not reproduce the in-vivo state of stress and strain of the material. Also, all these tests have been performed on ex-vivo myocardial specimens. But, soon after death, the rigor mortis causes a stiffening of the cardiac muscle which can influence the test results. For these reasons some recent works proposed an in-vivo material characterization using essentially cardiac imaging techniques, but, even if this seems the most powerful way, a standard and reliable method has not been defined yet [65, 66].

In this work, some assumptions were made to simplify the myocardium modelling without disregarding the main features of the cardiac tissue. First of all, the ventricular wall was considered as made of an incompressible material. In fact, the main constituent of the heart cells and the extra-cellular fluid is the water. The volume changes in the ventricular wall viewed as a continuum are due mainly to the fluid shift in the coronary vessels: during the diastole, blood flows into the coronary system thus producing an increase in the muscular volume; conversely, during the systole blood is squeezed out from the coronary vessels by the heart contraction, and the muscular volume decreases. But, since the coronary system modelling is out of the aims of the present thesis, the approximation of an incompressible material is justified, as in the majority of the literature works.

Furthermore, the application of the hyperelastic theory do not consider the viscoelastic properties of the myocardium. In fact, even if a viscoelastic behaviour of the cardiac tissue is present, it is not significant for the time range of the heart cycle, which is small with respect to the relaxation time [60, 67]. Also, the available data are very few, thus encouraging to treat the material as elastic.

Finally, for the cardiac tissue a transversely isotropic constitutive law was considered. Actually, the literature experimental findings suggest for the myocardium an orthotropic behaviour [60]; the orthotropic characteristic of the cardiac tissue is also suggested by the tissue microstructure, where the collagen fibres show different arrangement in the s_0 and n_0 directions (section 3.2.1, Figure 3.7). Nevertheless, the main features of the myocardium are well represented also by a transversely isotropic material. In addition, the identification of the material parameters is critical and not always supported by an adequate number of experimental data. The choice of a transversely isotropic material allows the optimization of the less possible number of parameters getting the characteristic stiffening in the myocytes direction.

_____

In the following sections the specification of the strain energy function for the passive and the active behaviour of the cardiac tissue will be presented, as well as the parameters identification.

Passive behaviour of the myocardium

The strain energy function selected to model the cardiac tissue was derived from Gasser, Ogden and Holzapfel [68]. The formulation of the strain energy is based on the invariants theory [69]. To model the anisotropic behaviour of the material, in addition to the three isotropic invariants described in Eq. (3.3), an additional quasi-invariant is needed. This quantity is related to the transverse isotropy of the myocardium, where the preferential direction along the myocytes axis, denoted as $\boldsymbol{f_0}$ in the reference configuration, is present. Let the fourth invariant of $\boldsymbol{C}$ be

$$I_4 = \boldsymbol{f_0}\cdot(\boldsymbol{Cf_0}) \qquad .$$

(3.15)

Note that this invariant is not affected if the fibres axis is reversed $(-\boldsymbol{f_0})$. In the invariant formulation, the strain energy function depends from a list of invariants $\psi = \psi(I_1, I_2, \dots, I_N)$; hence, Eq. (3.10) can be expanded as

$$\boldsymbol{\sigma} = \boldsymbol{F}\sum_{i=1, i\neq3}^{N}\frac{\partial\psi}{\partial I_i}\frac{\partial I_i}{\partial \boldsymbol{F}} - p\boldsymbol{I}$$

(3.16)

with the index 3 omitted from the summation because the material is incompressible.

Following Eq. (3.13), the deviatoric part of the strain energy is equal to the sum of an isotropic and an anisotropic contribution; the isotropic term refers to the collagen matrix which bounds the myocytes, while the anisotropic term refers to the myocytes mechanical contribution. Thus, the specialized forms of the two terms are equal to

$$\psi_{iso} = C_{10}(\overline{I_1} - 3) \qquad \psi_{aniso} = \frac{k_1}{2k_2}\{exp[k_2(\overline{I_4} - 1)^2] - 1\}$$

(3.17)

where $\overline{I}_1$ and $\overline{I}_4$ are the first and fourth invariants of $\overline{\boldsymbol{C}}$ respectively, and C_{10}, k_1, k_2 are the constitutive law parameters to identify. Note that the fibres contribution is active only if the fibres are stretched, while there is no anisotropic contribution if the fibres are compressed and the only isotropic matrix responds. The procedure used to assign the fibres orientation to the ventricular wall (section 3.2.1) basically defined the vector $\boldsymbol{f_0}$ which influences the material behaviour through the fourth invariant $\overline{I}_4$.

A formulation of this constitutive relationship is already implemented in the commercial code Abaqus. In Abaqus, a more complete equation of the Holzapfel-Ogden anisotropic model is available. In particular, the anisotropic part of the strain energy function is written as:

$$\psi_{aniso} = \frac{k_1}{2k_2}\sum_{i=1}^{N}\{exp[k_2(\langle\overline{E_\alpha}\rangle^2 - 1)^2] - 1\}$$

$$(3.18)$$

$$\langle\overline{E_\alpha}\rangle = k(\overline{I}_1 - 3) + (1 - 3k)(\overline{I_{4_{\alpha\alpha}}} - 1)$$

$$(3.19)$$

In Eq. (3.18) the summation over the index i allows the possible presence of more than one family of fibres; all the fibre families have the same mechanical properties (i.e. the same k_1, k_2) but can be characterized by different orientations, specified in the fourth invariant. In the myocardium, only one family of cardiac fibres was considered and the myocytes orientation was changed assigning at each layer of the ventricular wall a different fibre axis $\boldsymbol{f_0}$ (section 3.2.1). In this way it is possible to reproduce a realistic tissue structure, which exhibits one myocytes preferential orientation within each muscular sheet only. Moreover, the term $\langle\overline{E_\alpha}\rangle$ takes into account a potential dispersion of the fibre around the axis $\boldsymbol{f_0}$. Since the myocytes are essentially aligned in the muscular sheet this parameter was set to zero, meaning no fibres dispersion around the preferential direction. Hence, with these additional hypotheses, the anisotropic contribution of the strain energy function described by Eq. (3.17) was obtained.

Once the mathematical description of the material mechanical behaviour has been defined, the identification of the material parameters is required. The optimization of the coefficients C_{10}, k_1, k_2 was initially based on experimental literature data. In particular, the uniaxial mechanical tests performed on myocardium specimens by Ghaemi et al. [61] were considered. In the work of Ghaemi et al. ventricular wall

_____

samples of 5x5x0.15 mm were cut from bovine heart and tested under uniaxial and bi-axial load conditions. A specific protocol was developed by the authors to ensure the identification of the material preferential direction, i.e. the myocytes orientation. To fit the material coefficients on the stress-strain curves obtained by Gahemi et al., a routine was implemented in Matlab. In the algorithm, the explicit mathematical expression of the stress in the load direction was obtained for a uniaxial traction tests performed on a specimen with perfectly aligned myocytes. In particular, if the displacement is applied in the fibres direction $\boldsymbol{f_0}$, the stress in that direction has the form

$$\sigma_f = -p + 2C_{10}(\lambda^2 - \frac{1}{3}(\lambda^2 + \frac{2}{\lambda})) + 2k_1(\lambda^2 - 1)exp[k_2(\lambda^2 - 1)^2](\frac{2}{3}\lambda^2)$$

(3.20)

where λ is the applied stretch and p is calculated by imposing $\sigma_s = \sigma_n = 0$. Instead, if the displacement is applied in a direction perpendicular to the fibres like $\boldsymbol{s_0}$, the stress in the load direction is equal to

$$\sigma_s = -p + 2C_{10}(\lambda^2 - \frac{1}{3}(\lambda^2 + \frac{2}{\lambda}))$$

(3.21)

In Figure 3.10 a schematic representation of the two types of uniaxial tests modelled is given.
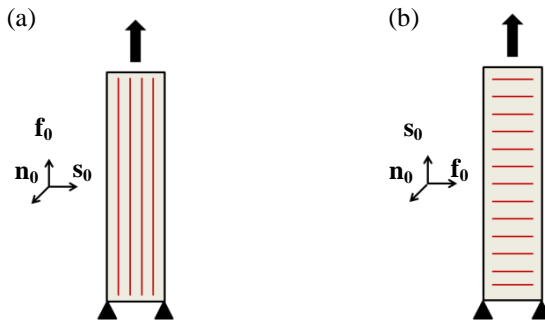

Figure 3.10. Schematic representation of the two types of simulated uniaxial tests: (a) the displacement is applied in the fibres direction; (b) the displacement is applied in the direction perpendicular to the fibres.

_____

Given the explicit forms of the stress, the material parameters were identified by fitting the experimental stress-strain relationships in the fibre and cross-fibre direction based on literature uniaxial traction tests. The resulting coefficients values are reported in Table 3.4. Figure 3.11 shows the experimental and modelled material response.
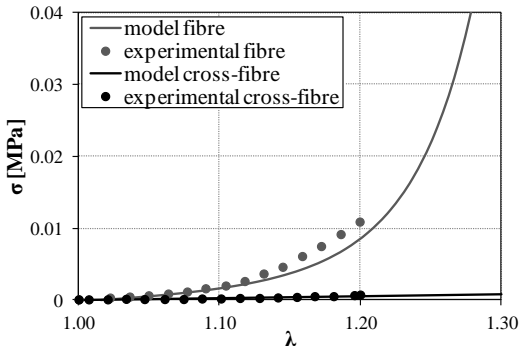

Table 3.4. Material parameterss obtained by fitting the constitutive model on the experimental data from Ghaemi et al. [61].

Parameter	Value
C_{10} [kPa]	0.2
k_1 [kPa]	3.1
k_2 [-]	5.35

Figure 3.11. Stress-strain relationship based on experimental data [61] (dots) and model results (solid line) in the fibre direction $\mathbf{f_0}$ and in the cross-fibre direction $\mathbf{s_0}$.

After the coefficients identification, the simulation of the ventricular diastole with the reference trabeculated model (section 3.1.2) was performed to validate the parameter estimation. Even if the material fitted quite well the experimental findings, the passive pressure-volume relationship didn't show an adequate behaviour. In particular, the resultant ventricular compliance was low with respect to the physiologic, and at a normal diastolic intra-ventricular pressure did not correspond a sufficient ventricular filling. The ventricular model was stiffer than the physiologic ventricle and even of a pathologic ventricle (Figure 3.12).
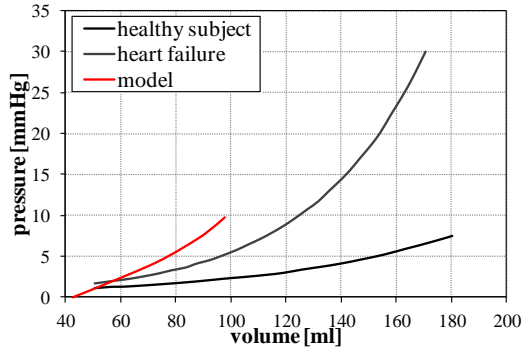
Figure 3.12. Experimental diastolic PV relationship of a healthy subject and of a heart failure patient [70], compared with the PV curve obtained by the simulation of the filling phase of the reference model characterized by the material parameters showed in Table 3.4.

Thus, a subsequent modification of the identified parameters was performed. Indeed, a realistic hemodynamic behaviour of the ventricle is fundamental for a correct evaluation of the differences induced by the presence of trabeculae at the endocardium, which is the main aim of this work. Starting from the coefficients values presented in Table 3.4, the parameters were scaled in order to obtain a physiologic ventricular compliance. A similar approach was recently adopted also by Krishnamurthy et al. [35]. Table 3.5 shows the scaled parameters values; note that a physiologic compliance was obtained by changing only the parameters related to the cardiac fibres. The scaled parameters were used to perform all the simulations, thus from now on, any reference to the material parameters will be related to the scaled parameters. Figure 3.13 shows the pressure-volume relationship of the trabeculated ventricle in diastole obtained with the two different set of parameters with respect to the experimental physiologic passive ventricular behaviour.

Table 3.5. Fitted and scaled parameters values.

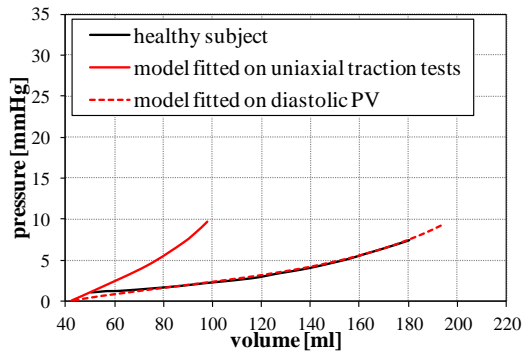| Parameter	Fitted Value	Scaled Value
C_{10} [kPa]	0.2	0.2
k_1 [kPa]	3.1	1
k_2 [-]	5.35	2

_____

Figure 3.13. Experimental diastolic PV relationship of a healthy subject [70] compared with the PV curve obtained by the simulation of filling phase of the reference model characterized by the material parameters showed in Table 3.5.

Active behaviour of the myocardium

During the systolic phase, the myocytes generate a contractile force secondary to an electrical stimulus. Normally, the electrical stimulus originates in the sino-atrial node, which lies between the superior vena cava and the right atrium (see Figure 1.1), and then propagates in all the cardiac chambers following a preferential pattern along the conduction system. While the membrane depolarization wave propagates, it causes the myocytes to be flooded by extracellular calcium, which regulates and sustains the contraction of the cardiac muscular cells; meanwhile, the extracellular matrix is passively subjected to the fibres contraction. The cardiomyocytes contraction produces, at a microscopic level, the fibres shortening and the stress increasing along the myocytes longitudinal axis; at a macroscopic level, these phenomena cause the blood to be ejected from the ventricle and the generation of the cardiac output. More in detail, the ventricular systole consists of different phases: the *isovolumetric contraction phase* is characterized by the muscular contraction without blood ejection, since both the inlet and outlet valves are closed. The intra-ventricular pressure increases, until the semi-lunar valves open to allow the blood ejection. This event marks the start of the *systolic ejection phase*, which concludes when the semi-lunar valves close secondary to a ventricular pressure fall (*isovolumetric relaxation phase*). After, the atrio-ventricular valves open, determining the beginning of the following heart cycle. Thus, to reproduce the ventricular systolic phase, two aspects must be considered: first, the myocytes contraction at the microstructural level; second, the presence of the fluid and the

cardiac valves which change the boundary conditions, contributing to the ventricular pressure and volume variation. In this section only the implementation of the material contraction is described, while the fluid cavity and the valves modelling will be presented in section 3.3 and 3.4.1.

As previously mentioned, the cardiomyocytes contraction produces an increase in the stress in the fibres axis and a shortening of the cardiac muscular cells. To take into account the muscular contraction, different approaches have been used in the literature. The most common is to add a contractile force in the stress tensor in the reference or current configuration (active stress model). This force is the result of the local electrophysiology on the cellular level [34, 37, 71]. In this work a different approach was adopted, similar to the one presented by Taber et al. [72]. In fact, the myocytes contraction and the consequent increase in stress was simulated by a stiffening of the material; this stiffening was obtained by changing the material parameters during the systolic phase. In particular, during the diastolic phase the material coefficients are constant and equal to the passive parameters. At the beginning of the systole there is an increase in the parameter values, which reach the maximum at about the 35% of the cardiac systole. Subsequently, these values decrease, returning to their initial values at the end of the systolic phase. The variation in the material coefficients follows the curve shown in Figure 3.14.
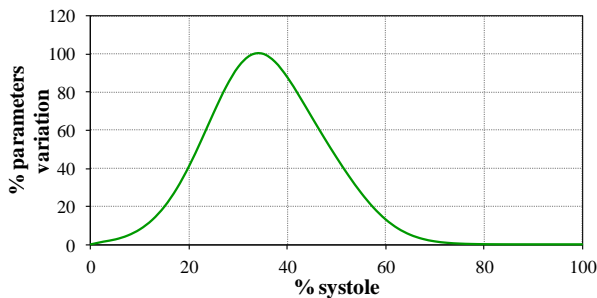

Figure 3.14. Percentage variation of material parameters during the systolic phase.

This curve was chosen with reference to the curve of force generated by a cardiac fibre due to an intracellular calcium variation [73]. The parameters change was imposed simultaneously to the whole ventricle, thus all the ventricular muscle contracts at the same time. Actually, the depolarization wave propagates with time, but this propagation is so fast in the ventricles that the heart is usually referred as a functional syncytium. Thus, for the aim of the present work, a simultaneous

_____

contraction of the whole structure was considered. Finally, the maximum material parameters in the systolic phase were found. In particular, the maximum coefficients values were chosen to obtain a physiologic torsional behaviour of the ventricle. The ventricular torsion is the mutual rotation of the ventricular base and apex (like the "the wringing of a linen cloth to squeeze out the water" [74]) which characterises the ventricular behaviour during systole. A positive torsion means a counter-clockwise rotation of the apex with respect to the base, viewing the ventricle from the apex (Figure 3.15).

Figure 3.15. Schematic representation of the ventricular twist. The ventricular torsion is defined as the difference between the apex angle of rotation (α) and the base angle of rotation (β) with respect to the ventricular axis.

The cardiac torsion is due to the fine interconnection of the cardiac wall components, and several studies have highlighted the sensitivity of this index to alterations in the wall mechanics [75–77]. Hence, a physiologic torsional behaviour, together with a physiologic pressure course, were considered as reliable indicators of the ventricular systolic modelling accuracy. The optimized diastolic and systolic maximum material parameters are shown in Table 3.6. The contraction force is mainly due to the stiffening of the myocytes, as reflected by the increase of the coefficient k_1.

Table 3.6. Diastolic and maximum systolic material parameters values.

Parameter	Diastolic Value	Maximum systolic value
C_{10} [kPa]	0.2	6
k_1 [kPa]	1	150
k_2 [-]	2	2

_____

3.3. VENTRICULAR CAVITY MODELLING

The basic mechanical parameters of the cardiac pump are the ventricular pressure and volume. The variations of these quantities during the heart cycle are due to the cardiac passive and active behaviour and to the boundary conditions. From the point of view of wall mechanics, the main boundary condition is the ventricular pressure, which depends both to the ventricular inward and outward fluid and to the muscular activity. To realistically model the pressure and volume variations in the ventricular cavity, a model of the ventricle should account also for the presence of the fluid in the cavity itself. The software Abaqus allows the simulation of fluid-filled cavities by means of a special type of elements called *hydrostatic fluid elements*. These elements provide the coupling between the deformation of the fluid-filled structure and the pressure exerted by the contained fluid on the boundary of the cavity. Hence, it is possible to model the mutual interaction of the ventricular cavity volume and pressure, as well to obtain the PV relationship of the ventricle. The hydrostatic fluid elements can be used only if the pressure and the temperature in the fluid cavity are uniform. Thus, any pressure gradient in the ventricle is disregarded. The hydrostatic elements are surface elements which cover the surface of the fluid-filled cavity. Some constraints have to be respected for a correct evaluation of the cavity volume. First, the fluid cavity must be closed. Hence, in all the models a surface was add at the ventricular base to close the fluid cavity. Further, where the cavity is delimited by structural elements, the hydrostatic elements must share the same node with the structural elements themselves, to allow the coupling between the displacement of the structure and the cavity volume change. In Figure 3.16, the ventricular fluid cavity is shown for the smooth and for a trabeculated model. Note that the node sharing was obtained by maintaining the same discretization for the ventricular inner surface and for the cavity.
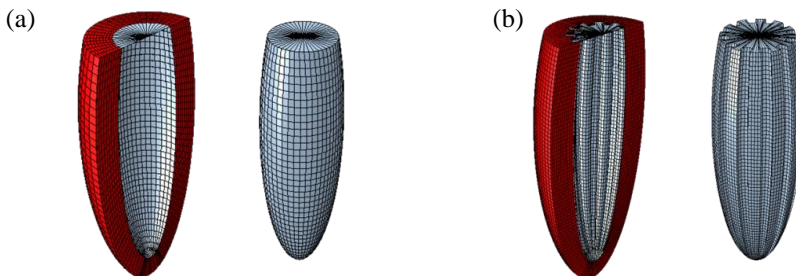

Figure 3.16. Axial section of the ventricular model (left) and ventricular fluid cavity only (right) for the smooth (a) and the trabeculated model(b).

_____

The fluid cavity volume is computed by the software through the definition of a reference node inside the cavity. Connecting the nodes which describe the cavity elements to the reference node, the hydrostatic fluid elements are no more surfaces but volumes, pyramidal elements. Furthermore, the element nodes must be connected such that the positive normal to the element surface points into the cavity. The positive normal is defined by the right-hand rule (Figure 3.17).
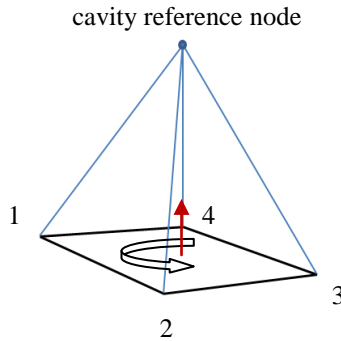
cavity reference node

Figure 3.17. Definition of a hydrostatic fluid element. The element nodes are enumerated such that the normal to the element (red arrow) pointed into the cavity. The volume is calculated by connecting all the element nodes to the cavity reference node.

For a faster implementation of the fluid cavities respecting all the described specifications a Matlab routine was developed. The routine implements the fluid element cavity having the nodes defined by the discretization of the ventricular endocardium as input.

The fluid was considered as incompressible, thus the fluid volume V doesn't depend on fluid pressure.

$$\frac{\partial V}{\partial p} = 0$$

(3.22)

The total fluid volume is the sum of the volumes of all the elements which constitute the cavity. Hence, to obtain V, the calculation of the volume of each element is needed. Let the element volume be V_e. The coordinates $\boldsymbol{x}$ of any point in the element depend on the nodal coordinates $\boldsymbol{x}^N$ and on the interpolation functions for the base of the pyramid N^N, expressed in terms of the parametric coordinates g and h

$$x = \sum_N N^N(g,h)x^N \ .$$

(3.23)

The infinitesimal volume dV associated to an infinitesimal area dA with normal $\boldsymbol{n}$ is given by

$$dV = \frac{1}{3}(x_R - x) \cdot \boldsymbol{n} dA$$

(3.24)

where

$$ndA = \left(\frac{\partial x}{\partial g} \times \frac{\partial x}{\partial g}\right) dgdh$$

(3.25)

$$\frac{\partial x}{\partial g} = \sum_N \frac{\partial N^N}{\partial g} x^N \qquad \frac{\partial x}{\partial h} = \sum_N \frac{\partial N^N}{\partial h} x^N \ .$$

(3.26)

and $\boldsymbol{x}_R$ are the coordinates of the reference node. The element volume is then obtained by integration

$$V_e = \int_{-1}^{+1}\int_{-1}^{+1} -\frac{1}{3}\overline{x} \cdot \left(\frac{\partial \overline{x}}{\partial g} \times \frac{\partial \overline{x}}{\partial g}\right) dgdh$$

(3.27)

where the relative position $\overline{x} = (x - x_R)$ has been defined. The variation in the element volume are consequently obtained by

$$\delta V_e = \int_{-1}^{+1}\int_{-1}^{+1} -\frac{1}{3}\left[\delta\overline{x} \cdot \left(\frac{\partial \overline{x}}{\partial g} \times \frac{\partial \overline{x}}{\partial g}\right) + \overline{x} \cdot \left(\frac{\partial \delta\overline{x}}{\partial g} \times \frac{\partial \overline{x}}{\partial h} + \frac{\partial \overline{x}}{\partial g} \times \frac{\partial \delta\overline{x}}{\partial h}\right)\right] dgdh \quad .$$

(3.28)

The hydrostatic elements also allow the modelling of a flow exchange between fluid cavities, which is useful in the definition of the preload and afterload circuits (section 3.4.1) and to simulate the diastolic and systolic blood flow. The cavities are characterized by their reference node, and the fluid transfer is possible by defining

_____

an element, called *fluid link element*, that connects the two reference nodes. The cavities can be physical entities, like the ventricle, or can be represented only by the reference node, where it is possible to apply pressure boundary conditions. The fluid mass flow q in the link element is considered as a homogeneous function of the pressure difference between the two cavities. Let the two cavities be identified by the indexes 1 and 2; the fluid mass variation Δm can be formulated as

$$\Delta m = q(\Delta p)\Delta t$$

(3.29)

where $\Delta p = p_1 - p_2$ is the pressure difference between the cavities and Δt is the time interval.

The fluid mass variation in a cavity due to the inflow or outflow is converted into a volume variation by means of the fluid density ρ:

$$\Delta V_1 = -\Delta m/\rho_1 \qquad\qquad \Delta V_2 = \Delta m/\rho_2$$

(3.30)

The fluid density was kept constant for all the cavities involved, and equal to 1000 kg/m^3. After the implementation of the fluid cavities, the only factor to be specified is the relationship between the mass flow rate and the cavities pressure difference $q(\Delta p)$. These function can be defined fixing some points of the function; a linear interpolation between the given values is considered.

For a detailed treatment refers to Abaqus Documentation [78].

_____

3.4. BOUNDARY CONDITIONS

During the beat, the heart is subjected to the action of various structures which surround the cardiac cavity and are connected to the heart itself. For example, the cardiac skeleton, the pericardial sac and the great vessels that originate from the heart chambers can influence the ventricular movements, limiting and constraining the heart displacements. In addition, the ventricular pressure depends on the ventricular preload and afterload, which consequently affects the performances of the ventricle. For an adequate model response, the modelling of both kinematic and pressure boundary conditions are needed. In the following sections the ventricular preload and afterload modelling as well as the kinematic constraints applied to the ventricular model are presented.

3.4.1. Preload and afterload circuits

In section 3.3 the ventricular cavity modelling has been described. The hydrostatic elements allow the simulation of a fluid at uniform pressure in the ventricular cavity. Since these elements permit also the simulation of a blood inflow and outflow from the fluid cavity, they were used to implement a preload and an afterload circuit for the ventricle. In particular, the modelling of a preload circuit is fundamental for the simulation of the diastolic phase, while an afterload circuit is needed for the simulation of the systolic phase.

During the cardiac diastole, the ventricular filling is due to the inflow of blood in the ventricle secondary to a pressure difference between the atrium and the intra-ventricular cavity. The mitral valve regulates this blood transition, ensuring a unidirectional flow from the left atrium to the left ventricle. Since just a functional modelling is desired, the complete modelling of the atrium and the valve structures is not necessary; thus, the atrium cavity was represented only by a reference node at a constant pressure. The atrium and the ventricular cavity were connected by a fluid link element, and the fluid flow was regulated by the function $q - \Delta p$ showed in Figure 3.18; $\Delta p = p_a - p_v$, where p_v is the intra-ventricular pressure and p_a represents the atrial pressure.
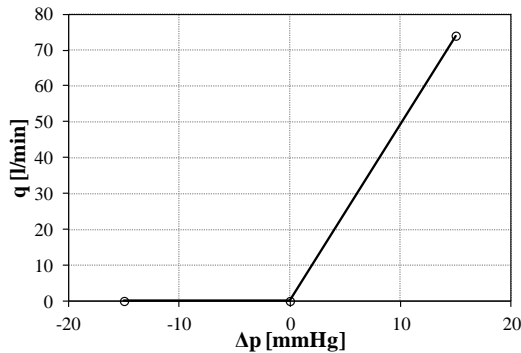
_____

Figure 3.18. $q - \Delta p$ relationship defined at the fluid link element which regulates the blood flow from the atrium to the ventricle.

The linear relationship between pressure difference and flow simulates a linear resistance placed between the ventricular and the atrial cavity (Figure 3.19). This resistance represents the mitral resistance to blood flow. The unidirectional flow was set by imposing zero flow for negative pressure difference. The left atrium reference node pressure was initialized at 5.25 mmHg during the first diastole and kept at this constant value for all the subsequent cycles. The ventricular filling starts when the intra-ventricular pressure drops under the atrial pressure; soon after the beginning of ventricular contraction the rising of the ventricular pressure above the atrial pressure value causes the stop of the inflow from the atrium, and establishes the end of the diastole.

Systolic phase is characterized by the myocytes contraction, which increases the ventricular pressure generating the cardiac output. The blood outflow depends on the characteristics of the systemic circulation, which includes the aorta and all the downstream vessels. If the afterload conditions change (e.g. an increase in the aortic pressure), this variation affects the ventricular pressure, and the ventricle adapts its performance to obtain a physiologic cardiac output. To model the afterload, a circuit composed by a resistance which represents the aortic resistance, in series with the parallel of a resistance and a compliance was developed (Figure 3.19). The parallel of a resistance and a compliance models in a simple but effective way the systemic circulation. Since Abaqus doesn't allow the mathematical modelling of compliances, the systemic compliant element was structurally implemented by defining a sphere of adequate diameter and stiffness [79]. This sphere is composed by shell elements with a thickness of 5 mm consisting of an isotropic elastic material; hydrostatic fluid elements were also add to model a fluid cavity. To guarantee a constant value of the

_____

compliance, the sphere dimensioning was performed under the hypothesis of small deformation (radius variation during the cardiac cycle lower than 1%). The resulting sphere diameter is equal to 208 mm, while the material young modulus and Poisson's coefficient are equal to 12 MPa and 0.3, respectively. To avoid rigid body motions of the sphere, an encastre was set at a single node of the structure. The circuit resistances and flow unidirectionality were modelled, similar to the preload circuit, by imposing a suitable piecewise linear function $\Delta p - q$ between the fluid cavities. Note that, besides the left atrium and the sphere cavities, the definition of another fluid cavity reference node was necessary to model the right atrium. The right atrium pressure was set at a constant value of 5 mmHg. Moreover, in the first simulated cycle the compliance cavity pressure was initialized at 80 mmHg in order to have a suitable ventricular downstream pressure during the first systole; this boundary condition was removed after the first cycle.
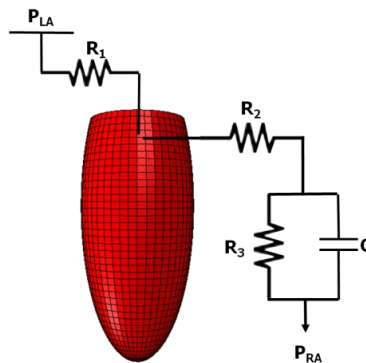

Figure 3.19. Electric analogue of the ventricular preload and afterload. (P_{LA}=left atrium pressure; P_{RA}=right atrium pressure).

The values of the resistive and compliant elements in the two circuits were optimized in order to obtain physiologic pressure curves in the ventricular and systemic compliance cavity reference node. The resulting values are consistent with the literature experimental data [80]. Referring to Figure 3.19, the pre and afterload circuit parameters values are summarized in Table 3.7.

_____

Table 3.7. Resistances and compliance values of the preload (R_1) and afterload (R_2, R_3, C) circuit (see Figure 3.20).

R_1 [mmHg*min/l]	R_2 [mmHg*min/l]	R_3 [mmHg*min/l]	C [l/mmHg]
0.2	0.375	18	0.0012

3.4.2. Kinematic boundary conditions

The left ventricular movements are restricted by many structures which surround the heart. Especially the ventricular base motion is affected by the constraint induced by various elements: the cardiac fibrous skeleton, composed by the connective tissue that constitutes and anchor the cardiac valves and that separates the atria from the ventricles; the aorta, which originates from the ventricle; the left atrium, which is directly connected to the ventricular base. To replicate the effect of all these structures on the ventricle, the models were constrained by preventing all the displacements of the nodes at the ventricular base, thus reproducing the limited motions of this portion of the ventricle (Figure 3.21).
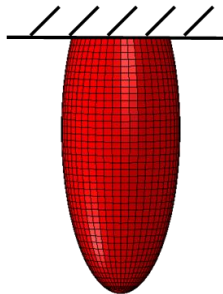

Figure 3.21. Kinematic boundary conditions of the ventricular models. All the displacements at the ventricular base were avoided.

The adequacy of this kinematic boundary condition was evaluated by analysing the model displacements during the heart cycle simulation in terms of longitudinal and radial displacements, as well as ventricular twist.

3.5. OTHER SIMULATION CONDITIONS

All the simulations were performed under the hypothesis of quasi-static processes. Thus, the pressure load varies during the analyses but the inertia effects are neglected. To confirm the validity of this assumption, a preliminary dynamic analysis was performed. The simulation results show that the kinematic energy is negligible with respect to the strain energy of the system, justifying the use of a quasi-static approach (Figure 3.22).
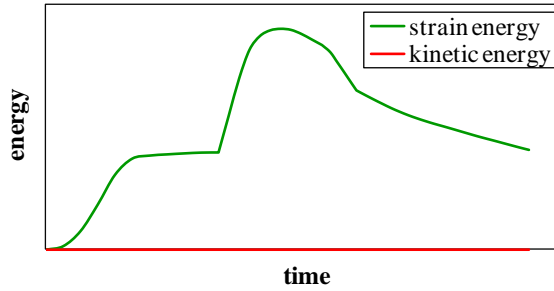

Figure 3.22. Strain and kinetic energy trend during a preliminary dynamic analysis for the ventricular model.

After the first cycle, when the atrial and aortic pressures were initialized and the end-systolic configuration for the ventricle was achieved, a minimum of four additional cycles were performed for each simulation to reach the steady state of the system. A standard cardiac frequency f of 75 bpm was considered. According to literature findings [81], the diastolic (T_D) and the systolic (T_S) period were calculated by the relationships

$$T_S = \sqrt{kT} \qquad\qquad T_D = T - T_S$$

$$(3.31)$$

where T is the duration of one cardiac cycle in seconds ($T = 60/f$) and $k = 0.096\ s$. Besides, to assess the influence of cardiac trabeculae on heart physiology, simulations at different cardiac frequencies were also performed changing the systolic and the diastolic duration according to Eq. (3.31). In particular three lower (10, 30 and 60 bpm) and two higher (110 and 180 bpm) frequencies with respect to the standard frequency were simulated.

_____

Chapter 4 :

RESULTS

In this chapter the results of the numerical simulation are presented. The comparison between the smooth and the trabeculated model outcomes are described in section 4.2, while the influence of trabeculae layer parameters are described in section 4.3. Finally, in section 4.4, the implications of the spongy myocardium presence on some aspects of heart physiology are shown.

_____

4.1. REFERENCE TRABECULATED MODEL

In this section the results of the reference trabeculated model are presented. As described in section 3.1.2, the reference model is characterized by: a trabeculated mass equal to the 15% of the total muscular mass, a trabeculae diameter of 4 mm and an apico-basal orientation of the trabecular structure. Since this model is the reference one, it should provide physiologic results in terms of hemodynamic outcome, as well as wall mechanics and kinematics, in order to allow an adequate comparison with the other models.

4.1.1. Hemodynamic outcomes

The main role of the left ventricle is to provide an adequate CO to the systemic circulation to ensure the blood perfusion of all the body compartments. Therefore, to analyse the model results, the first aspect to consider is the hemodynamic outcome of the trabeculated reference model in terms of generated pressure and flow. In Figure 4.1 intra-ventricular volume and pressure variation during the cardiac cycle determined by the model are shown.
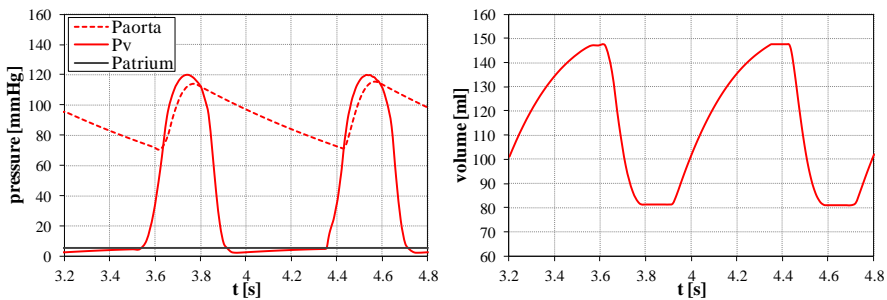

Figure 4.1. Left: pressure course in the ventricular cavity (P_v), the aorta (P_{aorta}) and the left atrium (P_{atrium}) during a cardiac cycle for the trabeculated reference model. Right: intra-ventricular volume variation during the cardiac cycle for the trabeculated reference model.

The reference model is able to reproduce the physiologic hemodynamic behaviour of the ventricle. The ventricular end-diastolic pressure is equal to 5.2 mmHg, while the systolic pressure peak reaches 120 mmHg. Further, the aortic pressure shows a physiologic trend: the maximum aortic pressure is about 115 mmHg, while the minimum is about 70 mmHg. Besides, the ventricular cavity volume shows an

_____

adequate variation during the heart beat: the EDV is equal to 148 ml, while the ESV reaches 81 ml. As a consequence of a physiologic variation of the intra-ventricular volume and pressure, the PV loop shown in Figure 4.2 was obtained for the reference trabeculated model.
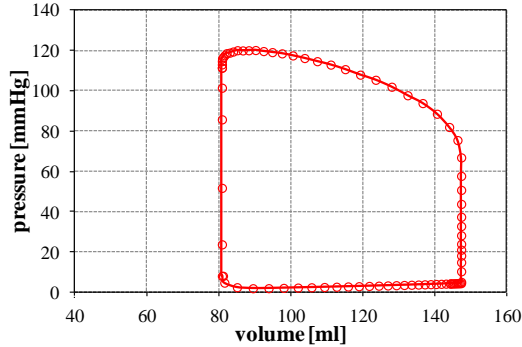

Figure 4.2. PV loop of the trabeculated reference model.

The ventricular SV is equal to about 65 ml; hence, at a frequency of 75 bpm, the trabeculated ventricle is able to generate a mean cardiac output of 4.9 l/min, a value close to the physiologic mean cardiac output, conventionally set at 5 l/min. This mean CO is the result of the dynamic variation of the outflow during the systolic phase. The instantaneous ventricular flow rate is represented in Figure 4.3. In this graph, the convention of a negative inflow in the ventricular cavity and a positive outflow from the cavity was considered. In particular, the negative flow represents the mitral flow rate, while the positive flow is the aortic flow rate.
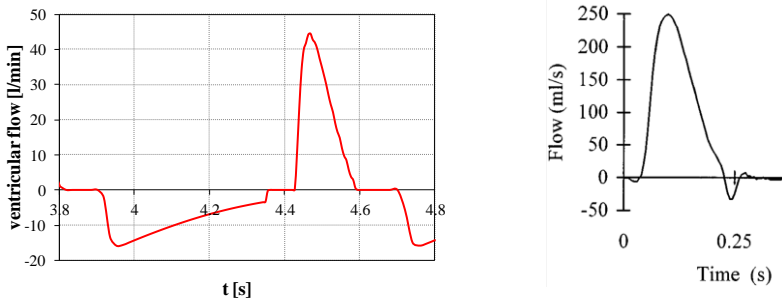

Figure 4.3. Left: ventricular instantaneous flow rate. A negative value indicates an inflow in the ventricle (mitral flow), while a positive value represents an outflow from the ventricle (aortic flow). Right: literature curve of the aortic flow in a dog [82].

_____

The ventricular flow rate curve is in good agreement with the experimental literature data; the two major differences are related to the outflow peak value and the inflow pattern. Indeed, the maximum outflow rate for an healthy subject at rest is about 25 l/min, while in the model the outflow peak is about 40 l/min [1]. Even if during exercise the physiologic CO increases to satisfy the increased body metabolic needs and can reach peak values of 40 l/min, this was not the case of the simulation at rest. This higher outflow peak can be explained by the absence of fluid inertia; since the presence of a real fluid in the cavity was not considered, no energy was spent by the ventricle to overcome the blood inertia, thus generating higher aortic flow peak.

About the inflow (or mitral flow), the curve trend for the reference model is different from experimental because of the absence of the atrial contraction simulation. In fact, the model filling is totally passive, due only to the constant pressure boundary condition at the left atrium reference node. Conversely, the experimental mitral flow curve exhibits a typical "two phase" filling pattern: the first phase refers to the early diastolic filling, when a rapid filling secondary to the sudden opening of the mitral valve occurs due to the maximum pressure difference between the atrium and the ventricle [83]. Then, when the pressure difference tends to vanish, the atrial contraction causes a second phase of rapid ventricular filling. Since the atrial contraction was not simulated and no atrial pressure dynamic was considered, the second filling phase cannot be recognized in the model outcome. Anyway, the end diastolic volume is physiologic, as well as the mitral flow rate mean value, highlighting an adequate simulation of the ventricular diastole for the study aims.

4.1.2. Kinematics

The analysis of the reference model displacements is important to understand if the model is able to replicate the physiologic ventricular kinematics. This is a fundamental aspect of the ventricular behaviour, since adequate wall motions are needed to ensure good ventricular efficiency. For this reason, the ventricular wall displacement velocities referred to the longitudinal and radial direction, as well as the ventricular twist are considered as indexes of cardiac performance in the clinical routine. In Figure 4.4 the comparison between simulated and experimental curves which represent the radial and the longitudinal velocity variation during the systole are shown. The diastolic phase was not considered since the totally passive ventricular filling is responsible for a different displacement dynamics of the ventricle. However, the order of magnitude and the displacement direction are respected also during diastole with respect to experimental data [84].

_____

The velocities were calculated in the model from the radial and longitudinal displacements of a node at mid-height of the ventricular axis. For an adequate comparison the results are presented in terms of systolic period percentage. Positive values of the longitudinal velocity means a ventricular extension, while a positive radial velocity indicates a cavity enlargement.
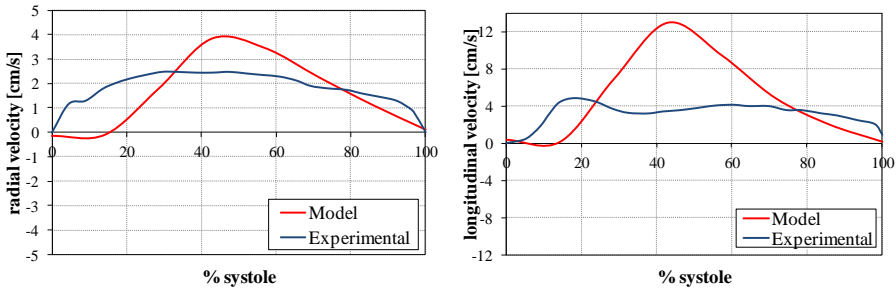

Figure 4.4. Radial (left) and longitudinal (right) velocity of the reference model during the systole compared with experimental literature data [85].

The radial and longitudinal velocity patterns in the model are consistent with experimental findings [85] in the systolic phase. However, the simulation results highlight a higher peak velocity in both the radial and longitudinal direction. These differences in the ventricular displacement velocities, both in the diastolic and in the systolic phase, are directly related to the different ventricular flow pattern for the model against the physiologic flow pattern. In fact, it's clear from Figure 4.5 that in the model the displacements velocities in both the analysed directions follows the ventricular flow trend. Hence, the differences in the ventricular flow are related to the variation in the ventricular displacement rate between the simulated and the real case: a higher outflow peak generates larger values of the longitudinal and radial velocities during the cardiac contraction, while the absence of a physiologic inflow pattern is responsible for a different course of the diastolic velocities.
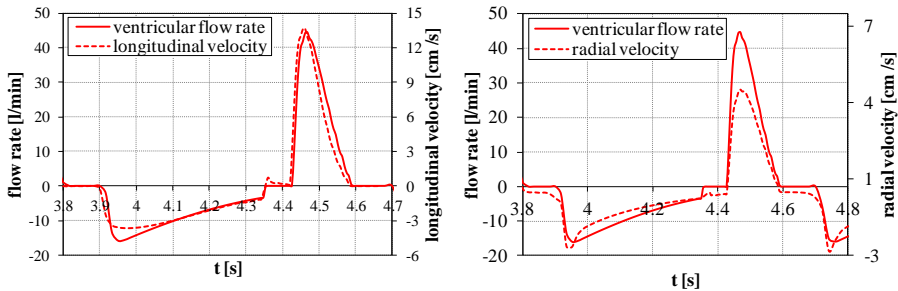
_____

Figure 4.5. Ventricular flow rate (solid line) and displacement velocity (dashed line) during the cardiac cycle for the reference model. Left: longitudinal velocity. Right: radial velocity.

During the cardiac cycle, the ventricular behaviour is not only characterized by a radial and a longitudinal displacement but also by a torsional movement (section 3.2.3) of the ventricular apex with respect to the base. In the literature several studies have been proposed for the analysis of the cardiac twist during the cardiac cycle, highlighting the validity of this parameter as an index of heart physiology [75, 76, 86–90]. Moreover, several model studies have revealed how ventricular torsion, which is primarily due by the complex fibres arrangement in the cardiac wall, is fundamental to obtain an adequate ventricular blood ejection and a uniform myocytes strain [72, 91, 92]. The reference model twist pattern during the heart cycle is presented in Figure 4.6, compared to experimental literature measurements. A positive value of the torsion is due to a counter-clockwise rotation of the apex with respect to the base, viewing the ventricle from the apex. On the contrary, an apex clockwise rotation is indicated by a negative value of the twist angle (Figure 3.15).
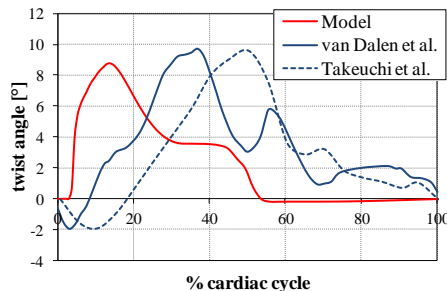

Figure 4.6. Comparison between the ventricular model twist and two experimental measurements of ventricular twist [76, 90] during the cardiac cycle.

_____

The model torsional behaviour is consistent with experimental findings in terms of twist pattern: during the systolic phase the apex undergoes a counter-clockwise rotation with respect to the base, generating a positive torsion; during the isovolumetric relaxation and the filling phase the ventricle recovers the systolic torsion, going back to the initial position. Even if the majority of the literature studies agree with this general behaviour of the cardiac twist during the heart beat, different torsional values can be found among different works. In this context, is difficult to find an optimal reference curve for the comparison with the model outcomes. Anyway, the ventricular model is characterized by a twist behaviour which reaches it maximum value too early in the cardiac cycle with respect to experimental findings. In particular the peak occurs at the end of the isovolumetric contraction, while in the heart the torsion peak is coincident with the aortic valve closure. Again, this difference between the real and the simulated behaviour can be influenced by the ventricular outflow pattern; indeed, the twist peak almost coincides with the aortic flow peak, highlighting the strong coupling between the model kinematics and the simulated blood ejection phase. Conversely, the maximum twist angle of the ventricular model is in the physiologic range (8° [93]-16° [86]).

Despite the differences between the physiologic and the model kinematics, the general consistency of the model outcomes in terms of radial, longitudinal and twist behaviour ensure the reliability of the reference model for the comparison with the other models.

4.1.3. Wall mechanics

The analysis of wall mechanics is fundamental in the developing of a reliable ventricular model. To evaluate the ventricular mechanics, in literature several studies have been presented to measure the ventricular wall deformations. On the contrary, literature data about experimental stress measurements are basically missing, and the stress distribution in the heart wall is usually investigated by computational approaches.

Many authors have measured the ventricular deformation *in-vivo* by means of different methods like imaging techniques, piezoelectric crystals and implantable beads [94–98]. In particular, two different reference systems are usually considered for strain calculations: the principal reference system, which almost lie in the circumferential, longitudinal and radial direction [94], and the strain in the coordinate system related to the fibres direction (i.e. the fibre, cross-fibre and

_____

normal direction, cfr. section 3.2.1, Figure 3.7), in order to analyse the myocytes deformation during the cardiac cycle and through wall thickness.

The comparison between the model strains and experimental data [95] in terms of longitudinal, circumferential and radial deformation are presented in Figure 4.7.
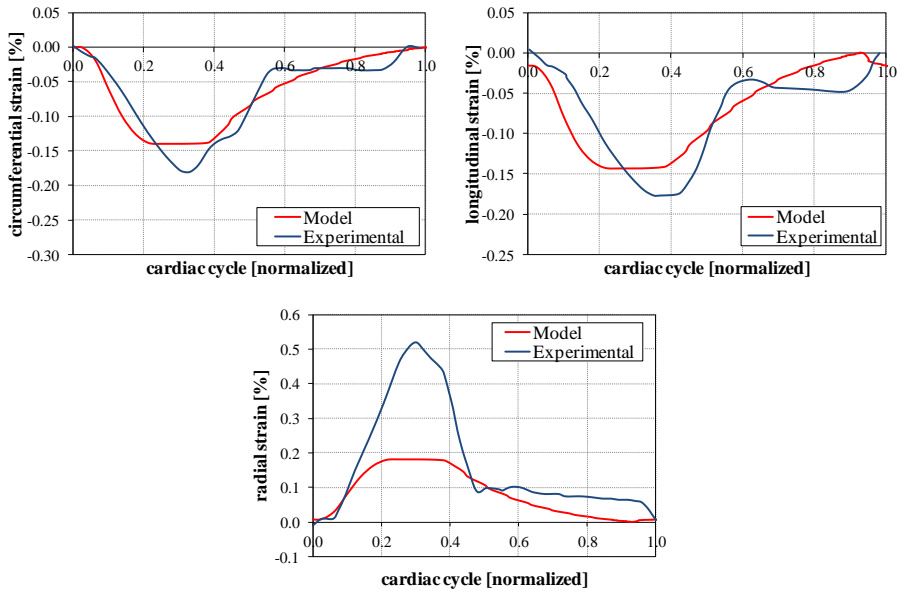

Figure 4.7. Comparison between the model circumferential, longitudinal and radial strain and experimental literature data [95].

While the model circumferential and longitudinal strains show similar pattern and values with respect to experimental data, the radial strain exhibits a trend consistent with the in-vivo measurements but a lower maximum value during the systolic phase. However, other values of the radial strain can be found among different authors, while there is a good agreement in the strain pattern within different studies. For example in Waldman et al. [94] the maximum radial strain is equal to about 0.3, while Langeland et al. [99] reported a maximum value of about 0.25, similar to what has been found for the reference trabeculated model.

Furthermore, the strains along the fibre direction were investigated. The analysis of the fibre strains is important since the myocytes contraction strongly depends on the stretch of the cardiac fibres during the passive ventricular filling. Indeed, the

_____

interconnection between the actin and myosin filaments is efficient only if the sarcomeres are stretched at an optimum level which is about the 10-15%. In Figure 4.8 the experimental and numerical strain distribution along the wall thickness are shown. The strains are referred to the end-diastolic state in the intra-trabecular spaces, taking the end-systolic state as reference.
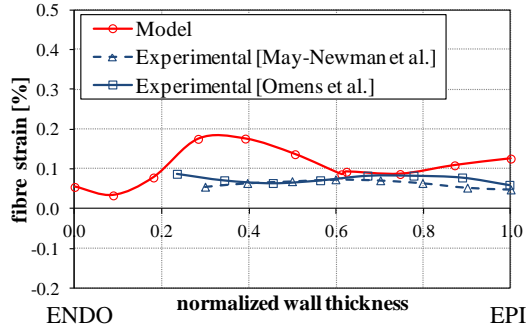

Figure 4.8. Experimental [100], [101] and numerical strain in the fibre direction along the wall thickness from endocardium to epicardium.

The model strain in the cardiac fibres direction is in any case in the standard deviation of literature experimental data [100, 101]. It's worth to be noticed that the myocytes strain is quite constant along the wall thickness, thanks to the characteristic cardiac fibres arrangement in the ventricular wall.

Since the model is able to reproduce a realistic distribution of the wall strains, the stress distribution obtained by solving the equilibrium problem is reasonable physiologic. In Figure 4.9 the fibre stress in wall thickness for the trabeculated model is represented. The presence of trabeculae makes the wall thickness not uniform; hence, for comparison purpose, the wall thickness was normalized and the stress distribution in both the trabeculae and in the inter-trabeculae spaces are shown. The stress are referred to a mid-axis ventricular section, at the systolic peak pressure time.
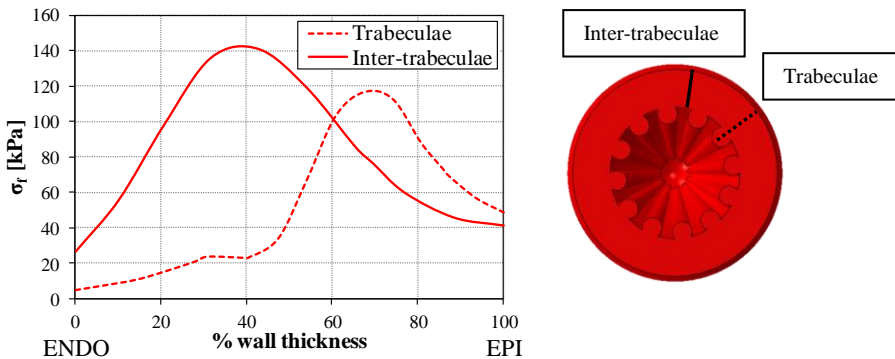
_____

Figure 4.9. Stress distribution along the wall thickness for the trabeculated model at two different sites (trabeculae, dashed line, and inter-trabeculae, solid line).

The stress distribution is influenced by the myocytes helical orientation in the ventricle: the maximum stress is reached in the inter-trabecular spaces at the mid-wall, where the wall thickness is lower and cardiac fibres are oriented circumferentially. On the contrary, at the epicardium and at the endocardium the fibre stress is minimum, because the myocytes are characterized by a oblique orientation with respect to the circumferential direction. This effect is even more evident at the trabeculae: the trabecular structures are oriented axially, as well as the cardiac fibres. As a consequence, the endocardial stress decreases much more on trabeculae than in the inter-trabecular spaces. A reduction in the stress at the endocardium is an advantage since this portion of the heart wall is the less perfused one. In fact, different studies have revealed how the myocytes arrangement can be useful to obtain a more homogeneous stress distribution in the heart wall [91, 92, 102], but the possible role of the trabeculae within this context has never been considered.

Note that the stress distribution during the systolic and the diastolic phase are nearly coincident, even if they are characterized by different values (Figure 4.10). Thus, the implemented contraction mechanism is able to replicate the Frank-Starling law: the myocytes which are characterized by higher stretch and stress during the passive filling are able to develop a higher contraction force.
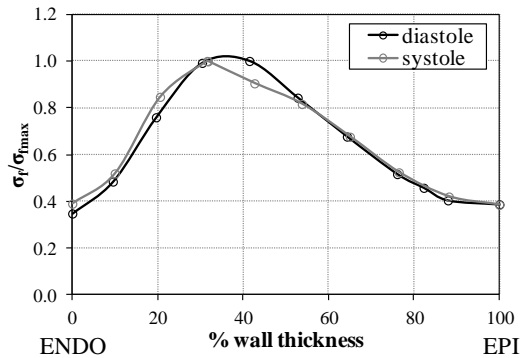
Figure 4.10. Stress distribution along the ventricular wall thickness at the end of the diastole and at the systolic pressure peak time.

4.2. COMPARISON BETWEEN THE TRABECULATED AND THE SMOOTH VENTRICLE

To investigate the influence of the presence of the spongy layer on the endocardial surface of the ventricle, the reference trabeculated model outcomes were compared with the outcomes of the smooth model. In this section the differences between the hemodynamic, kinematics and wall mechanics of the trabeculated and smooth model are presented.

4.2.1. Hemodynamic outcomes

Firstly, the intra-ventricular pressure and volume curves for the ventricle with and without the trabeculated layer were analysed. In Figure 4.11 the ventricular, aortic and atrial pressure are presented for both types of ventricle for the last two simulated cardiac cycles. At the same atrial pressure, and taking constant all the model parameters, the ventricular and aortic pressure for the trabeculated ventricle are significantly higher with respect to the smooth ventricle.
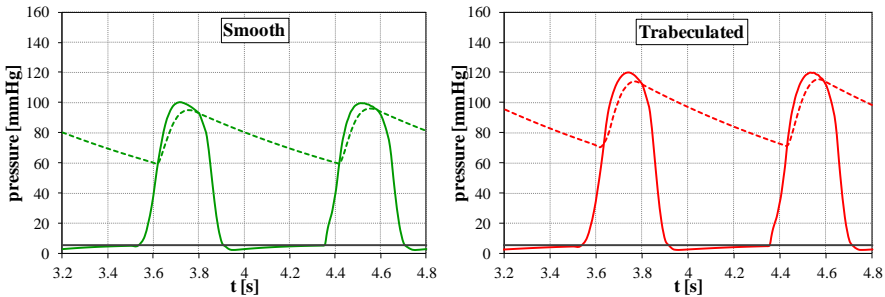
_____

Figure 4.11. Pressure curves for the smooth (left) and trabeculated (right) model. The solid lines represent the ventricular pressure, the dashed lines the aortic pressure and the grey solid lines the atrial pressure.

The raise in the ventricular systolic pressure, and the consequent increase in aortic pressure, are due to the higher EDV which characterizes the trabeculated model (Figure 4.12): at the same end-diastolic pressure, the EDV of the trabeculated model is equal to 148 ml, while the smooth model one is 113 ml. Hence, if the spongy layer is present, the ventricle exhibits a higher compliance. The larger ventricular filling volume causes an increase in the amount of blood ejected by the ventricle in the systolic phase. Indeed, according to the Frank-Starling law, a larger EDV means an higher myocytes stretch, which are consequently able to increase the developed force and SV. The instantaneous flow rate increases too (Figure 4.12), as well as the SV which is 54 ml for the smooth model and reaches 65 ml for the trabeculated model. Thus, at a constant cardiac frequqnacy of 75 bpm, the mean CO is equal to 4.9 l/min in the presence of trabeculae and 4 l/min in case of compact endocardium.
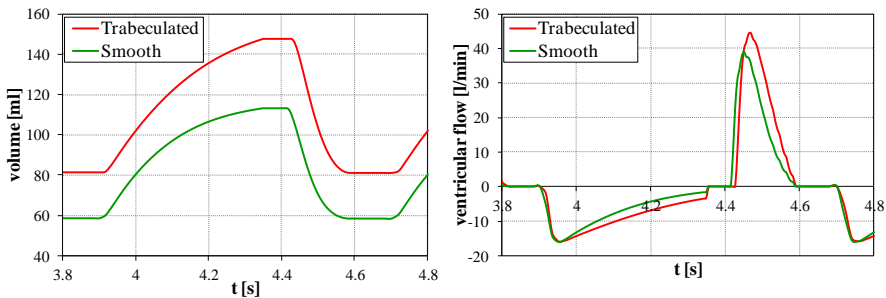

Figure 4.12. Ventricular cavity volume (left) and ventricular outflow (right) during the cardiac cycle for the trabeculated and smooth model.

_____

The differences in the trabeculated and smooth model behaviour are summarized in the PV loop of the two models (Figure 4.13).
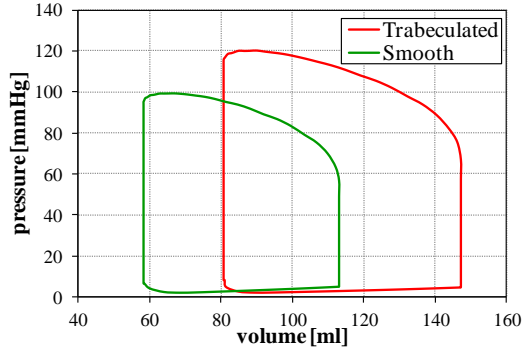

Figure 4.13. PV loop of the smooth and the trabeculated model.

The smooth model PV loop settles on the left side of the graph, which means lower ventricular volumes and pressures. Therefore, from a hemodynamic point of view, a trabeculated ventricle is able to guarantee better performances than a totally compact myocardium: the presence of trabeculae allows an easier ventricular filling, which induces the generation of a higher cardiac output for the systemic circulation.

4.2.2. Kinematics

To better understand the source of the ventricular compliance increase in the trabeculated ventricle, the radial and longitudinal displacements of the smooth and the reference model were calculated. In particular, the longitudinal displacement was measured at the ventricular apex, while the radial displacement referred to a section at the mid-ventricular axis (Figure 4.14).
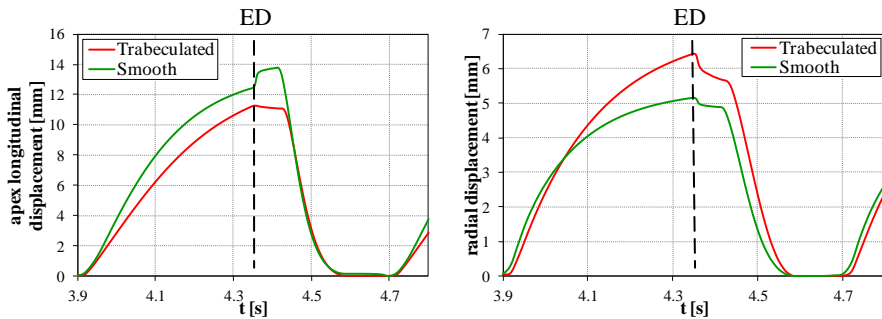
_____

Figure 4.14. Left: apex longitudinal displacement of the smooth and the trabeculated model. Right: radial displacement of the smooth and the trabeculated model. The dashed line indicates the end of the diastolic phase (ED).

The larger ventricular filling in the trabeculated case is due to a larger radial displacement during the diastolic phase; on the contrary, the longitudinal displacement is lower in the presence of trabeculae with respect to the smooth case. This displacement behaviour is probably caused by trabeculae orientation: since the trabecular structures are oriented along the axial direction, their presence limits the axial stretch of the ventricle.

4.2.3. Wall mechanics

The fibre strain in the trabeculated wall with respect to the fibre strain in the smooth wall at the end of the diastole is presented in Figure 4.15. The fibre strain was normalized in order to neglect the different EDV of the two models. For the trabeculated model, the fibre strain is referred to the inter-trabecular spaces.
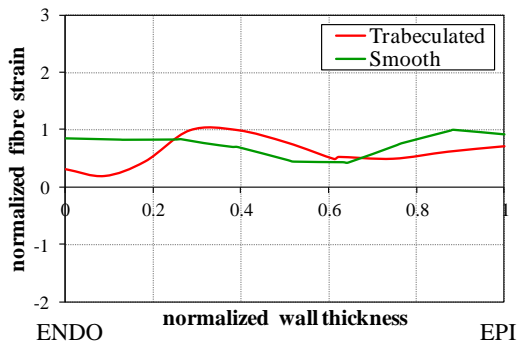

Figure 4.15. Normalized fibre strain along the wall thickness at end-diastole for the smooth and the trabeculated model.

_____

The trabeculated and the smooth model exhibit a quite uniform fibre strain distribution in the ventricular wall, and no significant differences can be recognized between the two cases. Also the radial, longitudinal and circumferential strains are similar in the trabeculated and smooth ventricle.

This similarity in the ventricular strains is reflected in the myocytes stress distributions in the wall thickness (Figure 4.16): the stress distribution in the compact layer of the trabeculated model is similar to the smooth ventricular stress pattern. The fibre stress was normalized on the maximum stress value to avoid differences due to the different EDV.
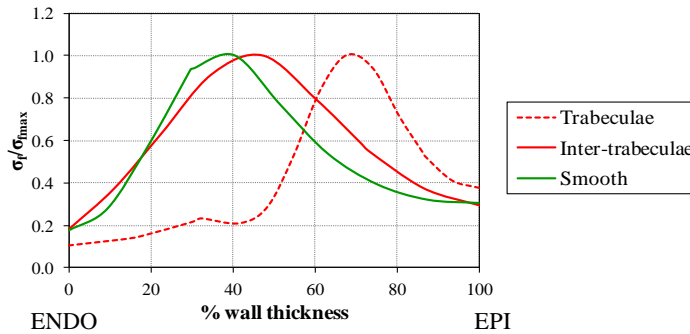
Figure 4.16. Stress distribution along the wall thickness at the systolic pressure peak for the trabeculated and the smooth ventricle. For the trabeculated case both the stress in the trabeculae (dashed line) and in the inter-trabecular spaces (solid line) are presented.

Therefore, the ventricular mechanics quantified by the ventricular stresses and strains is quite similar with respect to the smooth ventricle, while the presence of trabeculae strongly influences the model outcomes in terms of cardiac output and PV loop.

_____

4.3. INFLUENCE OF THE TRABECULATED LAYER PARAMETERS

In the previous section the trabeculated ventricle performance was evaluated against the smooth ventricle behaviour. The model outcomes can be dependent on the selected trabeculated layer parameters, like the trabeculae diameter and the trabecular mass. In this paragraph the comparison between models characterized by different trabeculated layer parameters is described.

4.3.1. Trabeculae diameter

Three different trabeculae diameters were implemented (section 3.1.2). The modelling of the fluid, which consists not in a fluid-dynamic approach but in the coupling between the cavity volume and a uniform pressure, is responsible for an identical hemodynamic behaviour at the different trabeculae size (Figure 4.17).
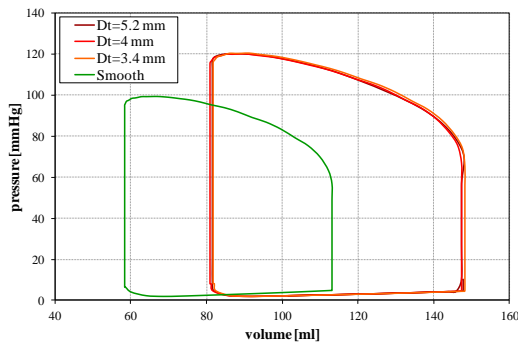
Figure 4.17. PV loop of the smooth and of the three trabeculated model with different trabecular diameter.

The ventricular PV loop doesn't change if a variation of the trabecular size from 3.4 to 5.2 mm is present; hence, the three different trabeculated models are able to develop the same cardiac output and are characterized by an identical trend of the intra-ventricular pressure and volume during the heart beat. As a consequence, also the displacement pattern of the different trabeculated models are nearly coincident, as demonstrated by the twist pattern during the cardiac cycle shown in Figure 4.18.

_____

Figure 4.18. Twist angle of the trabeculated models with different trabecular size.
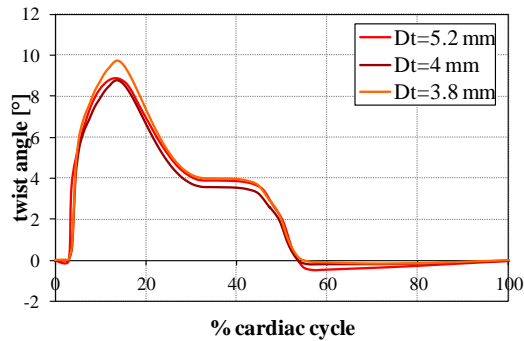
Nevertheless, the dimension of trabecular structure influences significantly the ventricular wall mechanics. Looking at the stress distribution between the endocardium and the epicardium, it can be pointed out that if the trabeculae diameter decreases, the stress distribution relative to the trabeculated case and the one relative to the inter-trabecular spaces tend to be closer (Figure 4.19). Note that the fibre stress in Figure 4.19 are not normalized since the EDV is the same for all the models, while the wall thickness was normalized to allow the comparison among different thickness. Therefore, the ventricular stress pattern shows that a reduction in the trabecular size is responsible for a more homogeneous stress distribution in the wall. The uniformity in the myocytes stress is fundamental from an energetic point of view: a homogeneous stress distribution suggests a uniform work and oxygen consumption of the cardiac fibres. In fact, even if the trabeculae diameter is variable in the normal ventricle, mostly the dimension of these finger-like structures varies in the range of a few millimetres.
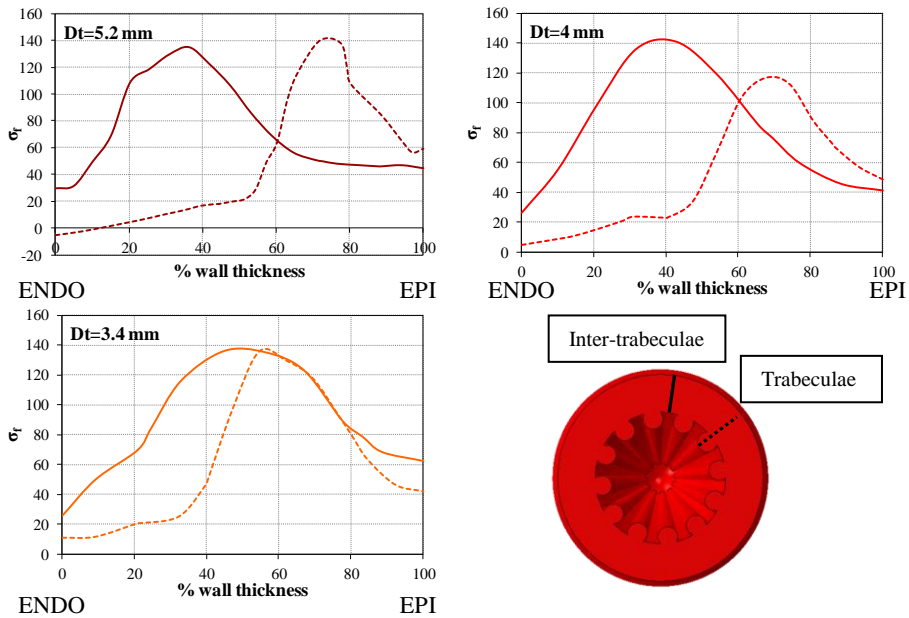
_____

Figure 4.19. Stress distribution at the systolic pressure peak along the wall thickness in the trabeculated models characterized by a diameter of trabeculae equal to 5.2 mm (brown line), 4 mm (reference model, red line) and 3.4 mm (orange line). The distributions referred to both the inter-trabeculae thickness (solid line) and the trabeculae thickness (dashed line) are shown.

4.3.2. Trabecular mass

Different trabecular masses were considered in order to analyse the influence of this parameter on ventricular performances. In particular, three trabeculated layer masses were implemented (section 3.1.2): in addition to the reference model trabecular mass (15% of the ventricular mass) the 7% and the 22% of trabecular mass with respect to the total muscular mass were considered.

The simulation results are first shown in terms of hemodynamic performances. The intra-ventricular pressure and the instantaneous flow rate during the cardiac cycle are presented in Figure 4.20; for comparison purpose, also the smooth model outcomes are shown. The ventricular pressure trend highlights how a larger amount of trabecular mass is responsible for a higher systolic pressure peak, even if this pressure raise is not significant from a clinical point of view (the pressure peak

_____

increases from 116 mmHg for a ventricle with the 7% of trabecular mass to 123 mmHg for the model with the 22% of trabecular mass). Consequently, also the flow rate curves obtained by the different trabeculated models are quite similar.
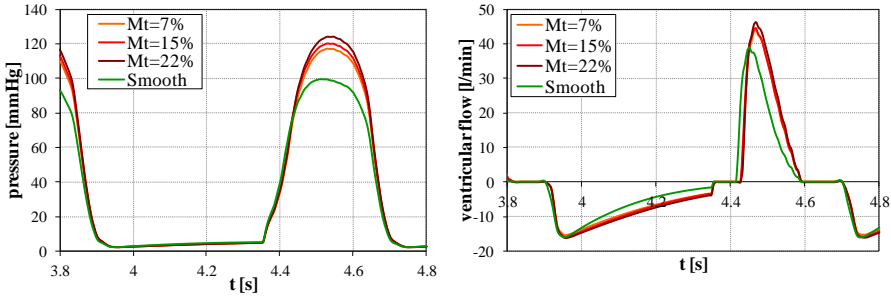
Figure 4.20. Ventricular pressure (left) and instantaneous flow rate (right) during the heart cycle for the trabeculated models at different trabecular mass (Mt) and for the smooth model.

An increase in the trabeculated models EDV causes the slight increase in the ventricular pressure during the systole (Figure 4.21, left). The EDV increase is proportional to the trabecular mass growth. The hemodynamic performances of all the trabeculated models at different spongy layer mass and of the smooth model are summarized by the PV loops in Figure 4.21 (right).

Figure 4.21. Ventricular cavity volume variation during the cardiac cycle (left) and PV loops (right) for the trabeculated models at different trabecular mass and for the smooth model.

The differences between the ventricular hemodynamic behaviour in case of a smooth ventricle and in case of a trabecular mass of the 7% are significantly higher with respect to the differences induced by a further increase of the spongy layer mass.

_____

Both the EDV and the SV exhibit a non-linear variation with respect to the trabeculated layer mass (Figure 4.22).
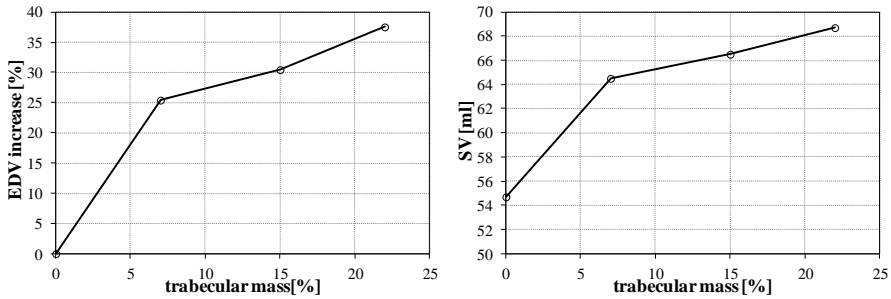
Figure 4.22. EDV (left) and SV (right) values against the trabecular mass variation for the different models. A trabecular mass of 0% represents the smooth case.

The same trend characterizes the CO, which increases from 4 l/min in the smooth ventricle to 4.875 l/min for a trabeculated mass of the 7%, and further increases to 5.175 l/min with the 22% of trabeculated mass.
A similar kinematic behaviour is also present in all the different trabeculated mass models, as shown by the twist pattern during the heart beat (Figure 4.23).
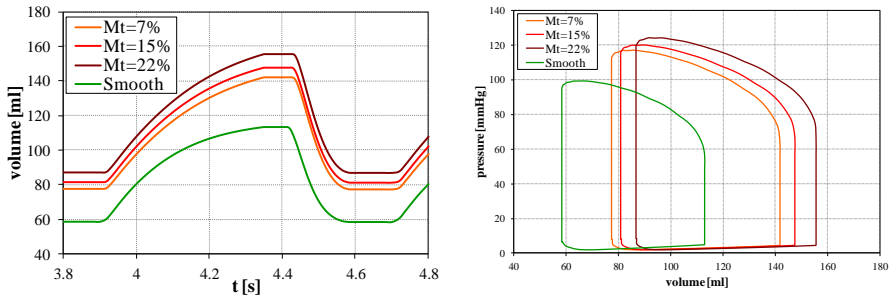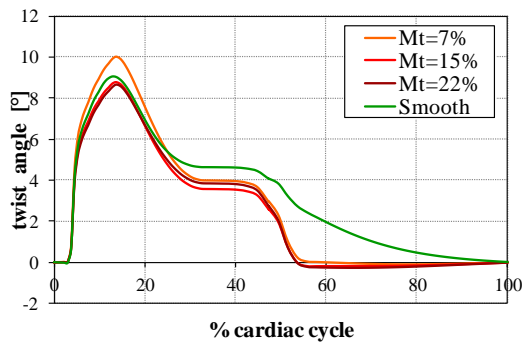

Figure 4.23. Ventricular torsion during the cardiac cycle for the smooth and the trabeculated models at different trabecular mass.

Therefore, an increase in the spongy layer mass around the physiologic range doesn't affect significantly the trabeculated model outcomes in terms of wall mechanics and hemodynamics. Nevertheless, an interesting trend was noticed in the

_____

ventricular EDV, SV and CO; the mere presence of a trabeculated mass is more relevant than the growth of the spongy mass, as demonstrated by the non-linear relationship between the trabecular mass and the hemodynamic parameters.

4.3.3.   Trabeculae orientation

All the results presented up to now were referred to trabeculated models with an apico-basal orientation of the trabecular structures. As described in section 3.1.2, an oblique orientation of the trabeculae at the endocardium was also investigated. In particular, the trabeculae were oriented at 60° with respect to the circumferential direction; the spongy layer mass in this model is equal to the reference one (15%). In Figure 4.24 the PV loops of the model with oblique trabeculation against the reference model (axial trabeculae, trabecular mass=15%) and the smooth model are described.
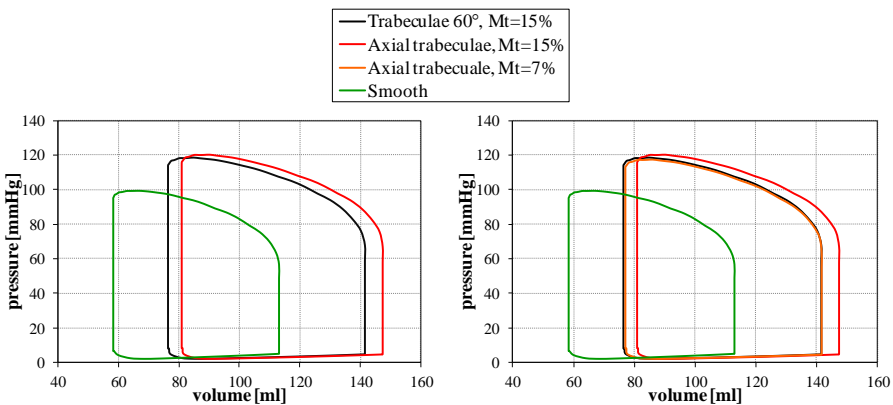
Figure 4.24. PV loops of the smooth model, the reference trabeculated model and the trabeculated model with a trabeculae orientation equal to 60° (left). On the right, also the trabeculated model with an axial trabeculated mass equal to the 7% of the ventricular mass is shown.

The inclination of the trabeculae at the endocardium doesn't affect significantly the intra-ventricular pressure and volume. The EDV is equal to 140 ml in the case of oblique trabeculae, against a ventricular filling of 147 ml for the reference model. Hence, the advantage in the ventricular compliance due to the presence of the trabeculated layer remains, even if a different trabeculae orientation is considered. However, the presence of a circumferential component of the trabecular arrangement

_____

tends to reduce this advantage: the macroscopic behaviour of the ventricle with oblique trabeculae is the same of the ventricle characterized by a smaller but axial trabeculated mass (Figure 4.24, right).

About the kinematic behaviour, the longitudinal and radial displacement and the twist of the ventricle with oblique trabeculae are shown in Figure 4.25, compared with the reference model outcomes.
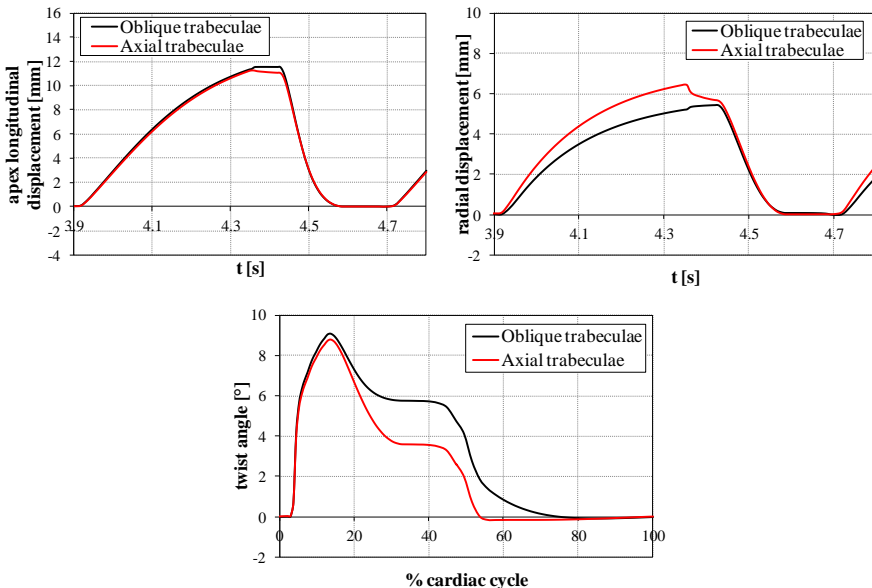
Figure 4.25. Ventricular longitudinal displacement, radial displacement and twist angle during the cardiac cycle for the model with axial and the model with oblique trabeculae.

While the longitudinal displacement is not affected by the trabeculae orientation, the radial displacement decreases if the trabeculae have an oblique direction. The consequence of this radial displacement reduction is the lower compliance which characterizes the PV loop of the model with non-axial trabeculation. Besides, the twist pattern is quite different in this model with respect to the reference model: after reaching the maximum torsion value, the recovery of the twist angle is slower in the ventricle with oblique trabeculae. Therefore, the inclination of the trabecular structure induces a slight decrease in the ventricular compliance and radial displacement, while changes significantly the twist pattern of the ventricle.

_____

All the results presented in this chapter up to now were obtained to meet the main aim of the work, namely the investigation of the role of the cardiac trabeculae on ventricular behaviour. These results have demonstrated the significant variations in ventricular performances if the trabeculated layer is present. Once this objective was reached, the possible influence of this different behaviour of the trabeculated ventricle on heart physiology was also investigated. In fact, the ventricle adapts its performances to satisfy the body metabolic needs, which change for example with the physical activity; the trabecular mass can potentially play a different role among the different work conditions. The results of this part of the work are presented hereinafter.

4.4. IMPLICATIONS ON HEART PHYSIOLOGY

As previously mentioned, the primary function of the ventricle is to generate an adequate cardiac output for the nourishment of all the body cells. The blood requirement of the body compartments is not constant with time, but it changes in function of the body activity. When this requirement increases, the ventricle must provide an higher outflow. Since the CO is obtained by multiplying the volume ejected in the single heart cycle by the cardiac frequency, an higher outflow of the ventricle can be achieved by acting on both these factors, namely the SV and the number of beats per minute. These two parameters are not totally independent: when the cardiac frequency increases, the diastolic and the systolic time change in a non-proportional manner. According to Eq. (3.31), the major variation occurs in the diastolic period, while the systolic time remains more constant even if the total cycle time decreases. Since the SV strongly depends by the EDV, when the heart rate increases at a frequency that doesn't allow the complete ventricular filling, this reduction in the EDV causes a reduction of the ejected blood volume. To assess the effect of heart rate on the behaviour of the trabeculated and the smooth ventricle, the simulations at different cardiac frequencies were performed. Further, some attempts to calculate the ventricular efficiency were made. Indeed, the efficiency is probably the most important parameter to investigate the ventricular performance, since it describes the ability of the ventricle to transform the incoming energy (namely, the myocardium oxygen uptake from the coronary circulation) into mechanical work (pumping action of the ventricle).

_____

4.4.1.   Effect of heart rate

In Figure 4.26 the PV loops of the trabeculated reference model at different cardiac frequencies are shown; in Figure 4.27 the same curves for the smooth case are presented.
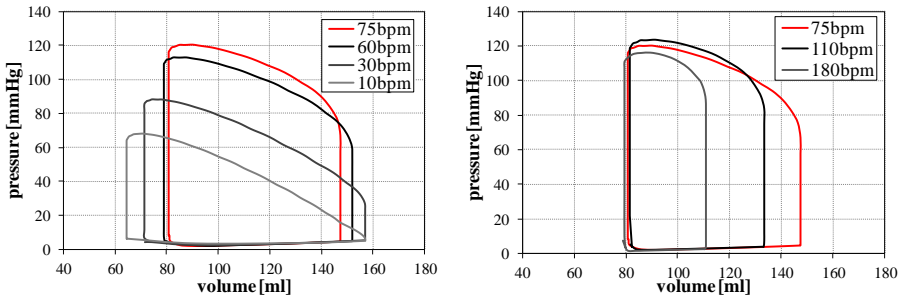
Figure 4.26. PV loops of the trabeculated reference model at different heart rate.
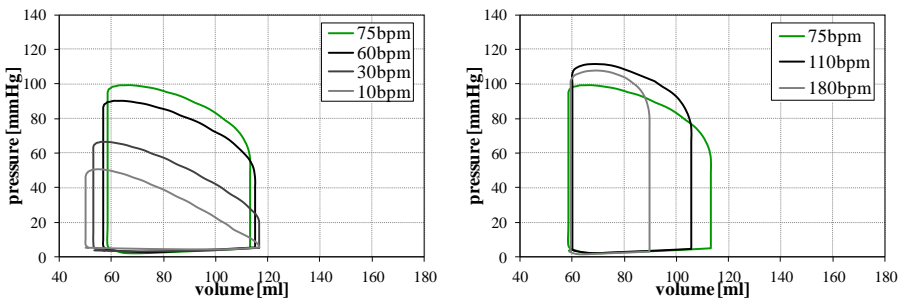
Figure 4.27. PV loops of the smooth model at different heart rate.

The pressure-volume loops just described for the trabeculated and the smooth model highlight a similar relationship between the ventricular hemodynamics and the heart rate for the two types of model. If the heart rate decreases below the standard frequency of 75 bpm (left side of Figure 4.26 and Figure 4.27), both the trabeculated and the smooth ventricle are characterized by an increase in the SV and a decrease in the systolic pressure peak. Conversely, if the heart rate is higher than the physiological one (right side of Figure 4.26 and Figure 4.27), a progressive reduction of the SV and a slight increase in the systolic pressure were obtained for

_____

both the models. These behaviours are consistent with physiological data, taking into account the consistency of the ventricular pre and afterload with the heart rate. But an essential difference in the behaviour of the smooth ventricle with respect to the trabeculated ventricle is present, as highlighted by the left-shift for all the heart rates of the PV loop of the smooth case against the trabeculated case. In fact, the trabeculated ventricle is able to guarantee an higher CO at each simulated heart rate. This higher CO is entirely due to an higher ventricular SV (Figure 4.28).
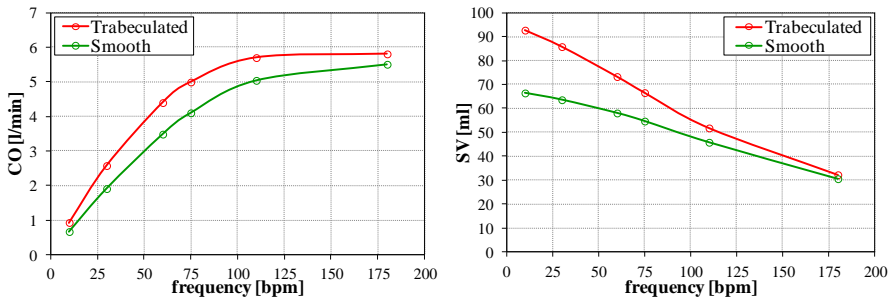
Figure 4.28. CO-cardiac frequency (left) and SV-frequency (right) relationships for the trabeculated and the smooth model.

The SV-cardiac frequency relationship is quite different for the smooth and the trabeculated ventricle: the curve slope for the trabeculated ventricle is higher with respect to the smooth ventricle. Hence, for the same variation of frequency, the trabeculated ventricle shows a more extensive variation of the ejected blood volume, and consequently an higher increment of the CO. Thus, in the trabeculated ventricle a wider regulation of the CO is possible.

_____

4.4.2. Ventricular efficiency

The ventricular efficiency is one of the most important index to evaluate the efficiency of the ventricle as a pump. Indeed, this index describes the amount of incoming energy which is converted into work used to pump the blood into the systemic circulation. From a mathematical point of view, the ventricular efficiency η is defined as

$$\eta = \frac{E_w}{E_{tot}} = \frac{\oint p dV}{E_{tot}}$$

(4.1)

where E_w represents the work and E_{tot} is the total energy incoming into the ventricle. In particular, the ventricular work is the area of the PV loop ($\oint p dV$), while the total incoming energy refers to the myocardium oxygen consumption. Typical values of physiologic ventricular efficiency are around the 10%, but this value changes with the body metabolic consumption [103]. Despite the relevance of this parameter in the evaluation of ventricular physiology, the efficiency is in general not considered in the clinical practice. Indeed, the oxygen consumption evaluation is not straightforward, and even if in the literature several methods can be found for the determination on the ventricular incoming energy, none of these methods is able to give a complete insight into all the different aspects which influence the efficiency of the ventricle. For this reason, in the following paragraphs the evaluation of the ventricular model efficiency with three different methods will be presented; the first two methods derive from experimental observations, while the third method refers to a mathematical method.

- *Method I*

Several studies have been reported a linear correlation between the myocardium oxygen uptake and the PVA (systolic pressure-volume area) [104], [105]. The PVA can be calculated by the PV loop as the sum of the ventricular work and the PA (Figure 4.29).

_____
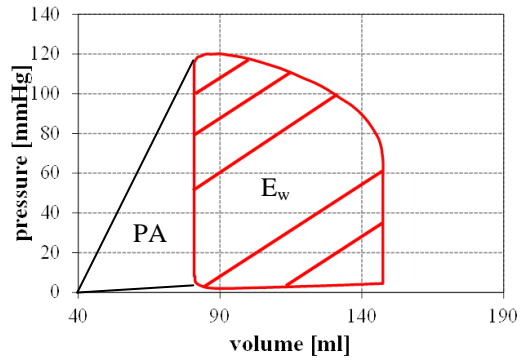
Figure 4.29. Definition of the work E_w and the PA for the calculation of the ventricular efficiency.

Hence, the Eq. (4.1) can be written as

$$\eta = \frac{\oint p\,dV}{PVA} = \frac{\oint p\,dV}{\oint p\,dV + PA} \ .$$

(4.2)

Based on this equation, the ventricular efficiency was calculated for the trabeculated and the smooth model at each frequency. As a result, the relationship between the efficiency and the CO was obtained for both models (Figure 4.30).
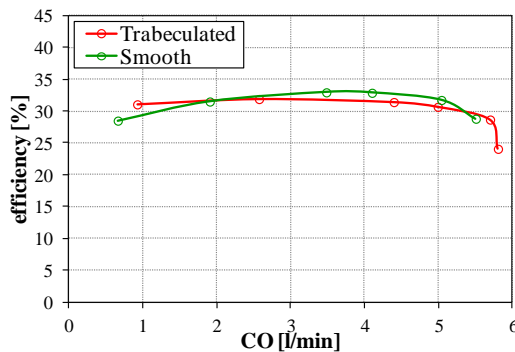
Figure 4.30. Ventricular efficiency-CO relationship of the smooth and the trabeculated model (*Method I*).

_____

The efficiency calculated with this first method is characterized by an higher maximum value with respect to the physiologic; the efficiency of the trabeculated and the smooth model are very similar, thus highlighting similar energetic performances for the two types of ventricle. Further, the efficiency is quite constant with the CO. Conversely, in the real case the efficiency shows a characteristic bell-type course against the ventricular outflow [106].

- *Method II*

The second method for the efficiency calculation takes into account the dependence of the myocardium oxygen consumption on the heart rate; in particular, to a higher cardiac frequency corresponds a larger oxygen uptake, which tends to decrease the ventricular efficiency. In the literature some studies have investigated the effect of the heart rate on the myocardium oxygen consumption [107, 108]. From these experimental data the ventricular efficiency was calculated at all the heart rates for the trabeculated and the smooth model (Figure 4.31).
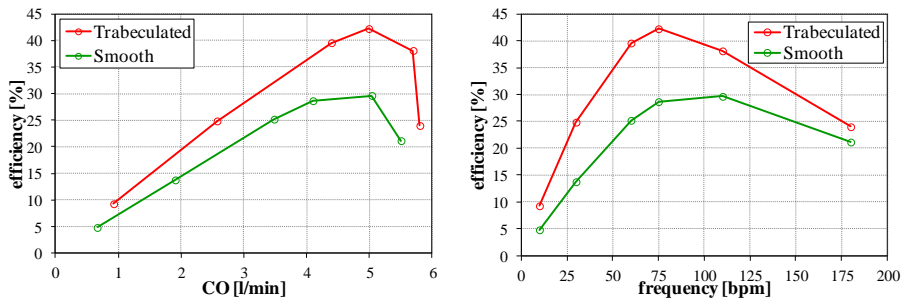
Figure 4.31. Ventricular efficiency-CO (left) and ventricular efficiency-cardiac frequency (right) relationships of the smooth and the trabeculated model (*Method II*).

In this second case, the efficiency-CO relationship shows a total different pattern with respect to the first method. First, the typical bell shaped curve was obtained; the maximum efficiency value was reached at the physiologic frequency of 75 bpm, but remains quite high also for heart rates around this value. Second, the smooth model is characterized by a significantly lower efficiency with respect to the trabeculated model. The highest difference can be recognized at the standard frequency of 75 bpm. Despite this, the ventricular efficiency values are still too high with respect to the physiologic. Thus, the use of this second method can explain why the

_____

achievement of the same CO with a lower frequency could be an advantage for the trabeculated heart; nevertheless, this conclusion cannot be reliable until the reasons of the non-physiological efficiency value will be completely understood.

- *Method III*

The last method for the determination of the ventricular efficiency is a mathematical method. It is well known that the ventricular incoming energy can be viewed as the sum of two terms: the first term relates as usual to the work; the second term is responsible for the amount of energy spent by the myocytes both to maintain their basal condition and to sustain the muscular contraction (*tension-time index, TTI*) [103]. In fact, the *TTI* accounts for the energy expenditure due to an isometric contraction; the latter is characterized by a constant length of the muscular fibre, and consequently at a macroscopic level this contraction doesn't generate a change in volume (namely no useful work). Nevertheless, the myocytes must spend energy to maintain the isometric contraction, and this energy is proportional to the fibre tension and to the contraction time. Hence, the efficiency can be defined as

$$\eta = \frac{\oint pdV}{\oint pdV + TTI} \qquad TTI = a \int_{t_s} Tdt$$

(4.3)

where T represents the fibre tension, t_s is the systolic period and a is a constant parameter. In the literature there is a lack of mathematical method for the identification of the fibre tension; the standard method consists in the experimental estimation of TTI from the aortic pressure curve [109]. But the implementation of a computational model has the fundamental advantage to provide the stress values in all the ventricular volume. Thus, to overcame the discrepancies which characterize the experimental methods previously described, an analytical formulation for the definition of the fibre tension was developed. In particular, the fibre stress σ_f was integrated in the ventricular volume and in the systolic time to calculate the TTI. Thus, the equation which describes the fibre tension was defined as

$$T = \int_V \sigma_f dV = \sum_{el} \sigma_{f\_el} * V_{el}$$

(4.4)

_____

where V_{el} is the volume of a single mesh element and σ_{f_el} the fibre stress pertaining to that element. Subsequently, the *TTI* was obtained by

$$TTI = a \sum_{t_s} \sum_{el} \sigma_{f\_el} * V_{el} * \Delta t$$

(4.5)

where the value of $a = 9 \ [1/s]$ was taken from a literature work [110] and Δt is the time interval. By means of that formula, the ventricular efficiency was calculated for the smooth and the trabeculated model (Figure 4.32).
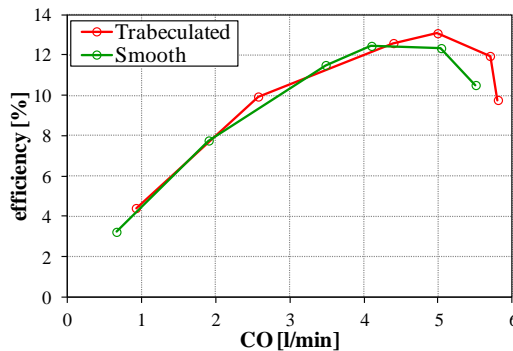
Figure 4.32. Ventricular efficiency-CO relationship of the smooth and the trabeculated model (*Method III*).

With this third method, as in previous case, the ventricular efficiency shows a bell trend, since the efficiency tends to decrease at low and high CO. The maximum efficiency value was reached at the physiological CO of 5 l/min for both the trabeculated and the smooth ventricle, putting in evidence the optimization of the implemented model to develop the physiological outflow. The smooth and the trabeculated ventricle show a very similar pattern, and no significant differences can be found between them in terms of efficiency. This third method is the only one among the three investigated methods which results in a physiological maximum value of the efficiency of the 13%.

_____

Chapter 5 :

DISCUSSIONS AND CONCLUSIONS

_____

5.1. DISCUSSIONS

In this work, a computational model to study the influence of cardiac trabeculae on ventricular behaviour was developed. The first step of the study was the optimisation of the trabeculated reference model in terms of hemodynamic outcomes and wall kinematics and mechanics. The simulation results highlighted the suitability of the reference model to simulate the physiologic ventricular behaviour: the model overall hemodynamic behaviour is consistent with experimental data, as well as the model kinematics and mechanics. Nevertheless, careful consideration must be given to the assumptions which were needed to develop the ventricular model. The main model hypotheses are summarized hereinafter.

1. *Geometrical model*: a simplified ellipsoidal geometry with a constant wall thickness was considered for the ventricle. Of course, regional variations in ventricular wall thickness and shape may influence the model outcomes in terms of local stress and strain, but the gross anatomy of the left ventricle is well described by the ellipsoidal geometry. Moreover, this geometry has allowed a parametric study to be performed on the trabeculated models.

2. *Cardiac tissue modelling*: some issues must be addressed regarding the material characterization. First, the passive material parameters were chosen by fitting the PV relationship of the structure during the diastole instead of optimising the material response on experimental data; in fact, the material optimization based on literature data obtained by mechanical tensile tests has demonstrated to lead to unrealistic hemodynamic outcomes. A realistic hemodynamic behaviour is fundamental for a reliable comparison between the reference and the smooth model. Nevertheless, the discrepancy between the structure and the material response highlights that the implementation of a suitable material constitutive law for the myocardium and the material parameters optimization is still an open issue. Secondly the active material behaviour was simulated by a stiffening of the material which permits to capture the main features of the systolic heart behaviour (e.g. the Frank-Starling mechanism), allowing an adequate comparison between the different models also during the blood ejection phase. Since the work was not focused on the microstructural characterization of myocytes contraction, the stimulus propagation during time and the cellular mechanism at the base of the myocytes contraction were disregarded (e.g. the dependence of contractile force on the intracellular calcium concentration).

_____

3. *Residual stress and strain*: the normal ventricle is characterised by the presence of residual stress and strain in the zero-pressure configuration. This residual stresses are the result of the myocardial growing and remodelling processes, and could influence the wall mechanics during the heart cycle. Despite this, an adequate experimental quantification of these residual stresses is not present in the literature, and this feature was not considered in the present model. The consistency of the reference model strains with experimental data ensures the validity of this assumption.

4. *Boundary conditions*: the ventricular displacements are limited at the base level by the presence of several structures like the great vessels and the pericardium. Hence, the encastre of the ventricular base was chosen as kinematic boundary for the models. Actually, the movements of the mitral valve plane are not completely avoided in the physiologic case, since all the structures are deformable. Even so, the reference model kinematics is in good agreement with the physiologic, showing the suitability of this boundary condition for a simple modelling of the heart constraints.

5. *Fluid inertia*: the lack of fluid inertia modelling may influence the model outcomes in terms of ventricular inflow and, especially, outflow, which shows a systolic peak significantly higher than the physiologic and, consequently, affects the ventricular kinematics (section 4.1.1). Despite this, the inclusion of the fluid inertia means the use of a fluid dynamic approach, which is beyond the objective of the thesis. Indeed, the adopted fluid cavity modelling permits to obtain all the hemodynamics quantity of interest (e.g. the PV loop, the ventricular and aortic pressure courses etc.), allowing an adequate comparison between the model performances.

6. *Preload*: the ventricular preload consists of a constant atrial pressure. Actually, the atrial pressure is characterized by a wave which varies during the cycle around the mean value. Anyway, the role of the atrial pressure in the model is only to achieve a physiologic value of ventricular filling. This result was obtained with the assumption of a constant atrial mean pressure, and consequently no pressure wave in the preload simulation was needed.

The assumptions just described refer to the modelling of the ventricle in general. Some other considerations should be done on the specific subject of the thesis, namely the modelling of a trabeculated ventricle in order to assess the influence of the spongy endocardial layer on heart performances.

_____

First of all, only the left ventricle was considered. In fact, the right ventricle shows a trabeculation which is apparently even more evident than the left ventricle, probably because of the smaller wall thickness, so it would be interesting to study the role of trabecular tissue also on the right ventricle. However, the left ventricle represents the major constituent of the ventricular mass and the heart chamber which has the preponderant mechanical role. Thus, the only left ventricle was modelled.

Secondly, regional differences in trabeculae dimension, shape and orientation were disregarded. The trabeculae were considered as cylindrical rods laying onto the endocardium to allow a parametric investigation of the trabeculae shape.

Once the reliability of the models were defined, some evaluation about possible differences in the efficiency displayed by the trabeculated and the smooth ventricles have been done. Even if this task was not present in the thesis aims, some brief considerations about this last part of the work have to be pointed out. Indeed, the ventricular efficiency is one of the most important parameters for the evaluation of heart performances. The use of different methods for the efficiency calculation have lead to different conclusions about the comparison between the trabeculated and the smooth ventricle outcomes. This has been mainly due to the lack of information about the myocardial oxygen uptake, which is necessary for the efficiency calculation. To overcome this problem, the oxygen consumption was estimated based on the computational model results. In this case efficiency didn't show remarkable differences between the two kinds of ventricles (trabeculated or smooth). Summarising, the three different approaches used to evaluate ventricular efficiency didn't allow to reach a conclusion. This opens new scenarios and encourages further investigations aimed at the deeper understanding of this fundamental aspect of the ventricular behaviour.

_____

5.2. CONCLUSIONS

In the study of heart behaviour, the presence of a trabeculated layer at the ventricular endocardium is almost disregarded, despite the evidences of a significant contribution of cardiac trabeculae on the physiologic ventricular performances. For this reason, aim of the thesis was to study the role played by trabeculae on the ventricular mechanics by a computational approach. First, the trabeculated reference model was developed. The reference model development has included several issues: the implementation of a physiologic trabeculated ventricular geometry; the modelling of the cardiac tissue, which accounts for a realistic fibre distribution and for an adequate material constitutive law of both the active and the passive material behaviour; the definition of suitable model boundary conditions; the modelling of the ventricular fluid cavity. The model was able to reproduce the physiologic hemodynamic, kinematic and mechanical behaviour of the left ventricle. Hence, it has been demonstrated to be a reliable reference for the comparison with the other implemented models.

The fundamental comparison was performed between the reference trabeculated model and a smooth model. The smooth ventricle was implemented keeping constant the total muscular mass and the intra-ventricular volume, in order to meet the specifications declared in the thesis objectives. This approach has guaranteed a reliable comparison between the two types of ventricle, which has highlighted a remarkable difference in the ventricular compliance in the presence of trabeculae. Indeed, the EDV shows a remarkable increase in the trabeculated ventricle with respect to the smooth (+30%), and consequently a larger SV during the systolic phase (+20%). The ventricular filling is a fundamental parameter in determining the heart performances; more than the 50% of the patients suffering of heart failure symptoms show a normal ejection fraction and are referred to as diastolic heart failure patients [111]. Moreover, diastolic dysfunctions can be recognized also in patients with systolic heart failure. In this context, the trabeculae play a fundamental role, since they can significantly contribute to the achievement of a physiologic EDV. Note that the advantage due to the presence of trabeculae is more evident in the diastolic phase than during the ejection phase. This difference may decrease if a contact between the trabecular structures was considered. In fact, the contact between trabeculae could lead to an increase in the ventricular wall thickness during the contraction phase, enhancing the systolic pressure generation. For this reason, we are working on a modification of the model presented in this thesis to account for this aspect of the ventricular behaviour.

_____

Further, the computational model has resulted suitable to perform a parametric study, which allowed the variation of trabecular mass, size and orientation. In particular, a non-linear dependence of the ventricular hemodynamics on the trabeculated mass was found: a higher trabecular mass is responsible for a larger compliance, but the main advantage in terms of ventricular filling is due more to the mere presence of trabeculation than to a progressive increase of the trabecular mass. In this work only a slight increase of the trabeculated mass above the physiological maximum value of the 20% was considered, and the corresponding EDV was in the physiologic range. However, based on the model results, it's reasonable to infer that further non-physiological increments of the trabecular mass would lead to an excessive increase of the ventricular filling, which would lead to heart failure. Thus, even if a greater insight into this pathological condition is needed, the present study opens interesting scenarios for the investigation of the LVNC pathologies, emphasising the importance of a physiologic balance between the compact and the spongy mass in the ventricle.

Furthermore, the model outcomes highlighted how the trabeculae diameter affects the stress distribution: the myocytes stress is more uniform in case of smaller trabeculae. This finding could explain the preferentially presence of fine trabeculations at the endocardium; indeed, the stress distribution uniformity is important for a homogeneous energetic consumption of the cardiac cells and, consequently, of a uniform myocytes work and oxygen demand.

Finally, the last part of the thesis suggests a possible role of the cardiac trabeculae on heart energetics. Since the trabeculated ventricle is able to guarantee the same CO at lower heat rate than the smooth ventricle, a higher efficiency could be reached by the trabeculated ventricle based on the dependence of the efficiency on the cardiac frequency, which has been reported in the literature.

To our knowledge, this is the first study focused on the analysis of the influence of the trabeculae on the ventricular mechanics. The computational approach adopted in the work has been demonstrated to be a reliable method to assess the significant influence of cardiac trabeculae on different aspects of the ventricular physiologic behaviour, laying the foundations for new approaches in the studies of this subject.

APPENDIX A

_____

RECONSTRUCTION OF THE VENTRICULAR INNER SURFACES

In Chapter 1 the lack of quantitative data about the structure of the cardiac trabeculae was emphasized. Indeed, experimental measurements of the trabeculae dimension, orientation and three-dimensional arrangement are mostly disregarded in the literature. For this reason, the quantitative analysis of the trabeculated ventricular surface was attempted as a starting point of the present work. Since the standard imaging techniques (e.g. magnetic resonance imaging, echocardiography) are characterized by an insufficient resolution for a correct trabeculae identification, a different approach was used. This method consisted in the *ex-vivo* reconstruction of the inner ventricular surfaces by means of a laser camera.

In the experimental protocol, a wild boar heart maintained in 50% formalin and alcohol solution was sectioned in six parts (dissection performed in collaboration with the Laboratory of Pathology, Fleming Institute, Milan). Each one of the six parts were scanned by a laser camera (Non Contact 3D Digitizer Vivid 9i/VI – 9i, Konica Minolta Optics Inc.) at the Reverse Engineering Laboratory of the Mechanical Engineering Department, Politecnico di Milano. The laser camera allows the acquisition and digitalization of an object surface with a plane resolution of 0.3 mm and a resolution in the direction normal to the plane of 0.09 mm. For each section some captures at different angles were performed, in order to acquire as much surface details as possible. Two cardiac samples and the respective acquisitions are shown in Figure A.1.

Figure A.1. Cardiac sections and relative laser acquisition.

The high complexity of the ventricular trabeculated surface didn't allow the exposition of all the surface details. The areas where the laser was not able to

_____

penetrate resulted in the presence of holes in the surface reconstruction. Hence, a post-processing was necessary to refine the laser acquisitions. A hand repair of the mesh surface was performed with Rhinoceros® to close the holes in the trabecular surface (Figure A.2).
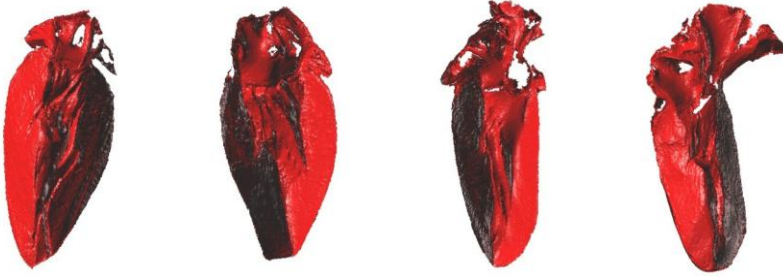
Figure A.2 Four acquired sections of the left ventricle after the hand repair of the surface mesh.

Both the right and left ventricular surfaces were acquired, but only the left ventricle acquisitions were processed. After the adequate repair of all the ventricular sections, the single parts were further elaborated to obtain the closed left cavity. The sections were merged with MeshLab (ISTI-CNR, Pisa, Italia), and the cutting planes and the atrial surface eliminated. Attention was paid to the merge procedure: the excised ventricle is not stress-free, but residual stresses are present in the cardiac wall. As a consequence, when the heart was cut a change in its shape occurred, and the different portions didn't matched perfectly after the sectioning procedure. Hence, the cutting planes were used for an easier individuation of the contact points between the different sections before the cutting planes removing. The result of the sections merge is shown in Figure A.3.

_____

Figure A.3. Final reconstruction of the left ventricular surface.

This reconstruction of the left ventricular cavity allowed a deeper understanding of the trabecular network arrangement, highlighting a preferential oblique orientation of the trabecular structures. This feature was employed for the implementation of one of the trabeculated model (section 3.1.2) in order to investigate the influence of trabeculae orientation on the ventricular response.

BIBLIOGRAPHY

_____

[1]   A. C. Guyton and J. E. Hall, *Textbook of Medical Physiology*, X Edition. W.B. Saunders Company.

[2]   F. H. Netter, *Atlas of Human Anatomy*, Fourth ed. Ed., John T. Hansen, 2006.

[3]   S. Goo, P. Joshi, G. Sands, D. Gerneke, A. Taberner, Q. Dollie, I. Legrice, and D. Loiselle, "Trabeculae carneae as models of the ventricular walls: implications for the delivery of oxygen.," *J. Gen. Physiol.*, vol. 134, no. 4, pp. 339–50, Oct. 2009.

[4]   G. C. Balboni, *Anatomia umana.* Edi.Ermes, 1991.

[5]   J. S. Frank and G. A. Langer, "The myocardial interstitium: its structure and its role in ionic exchange.," *J. Cell Biol.*, vol. 60, no. 3, pp. 586–601, Mar. 1974.

[6]   A. A. Young, I. J. Legrice, M. A. Young, and B. H. Smaill, "Extended confocal microscopy of myocardial laminae and collagen network," vol. 192, no. November, pp. 139–150, 1998.

[7]   G. Sands, S. Goo, D. Gerneke, I. Legrice, and D. Loiselle, "The collagenous microstructure of cardiac ventricular trabeculae carneae," *J. Struct. Biol.*, vol. 173, no. 1, pp. 110–6, Jan. 2010.

[8]   K. T. Weber, "Cardiac Interstitium in Health and Disease : The Fibrillar Collagen Network," vol. 13, no. 7, 1989.

[9]   D. D. J. Streeter, *Gross morphology and fiber geometry of the heart. In Handbook of physiology*. ed. R. M. Berne, N. Sperelakis & S. R. Geigert, 1979, pp. 61–112.

[10]   D. D. Streeter, H. M. Spotnitz, D. P. Patel, J. Ross, E. H. Sonnenblick, B. D. D. Streeter, and H. M. Spotnirz, "Fiber Orientation in the Canine Left Ventricle during Diastole and Systole," *Circ. Res.*, vol. 24, pp. 339–347, 1969.

[11]   G. B. Sands, D. A. Gerneke, D. A. Hooks, C. R. Green, B. H. Smaill, and I. A. N. J. Legrice, "Automated Imaging of Extended Tissue Volumes Using Confocal Microscopy," vol. 239, no. February, pp. 227–239, 2005.

[12]   F. Torrent-guasp, M. Ballester, G. D. Buckberg, F. Carreras, I. Carrió, A. Ferreira, L. E. Samuels, and J. Narula, "Spatial orientation of the ventricular muscle band: Physiologic contribution and surgical implications," *J. Thorac. Cardiovasc. Surg.*, vol. 122, no. 2, pp. 389–392, 2001.

[13]   F. Torrent-guasp, W. F. Whimster, and K. Redmann, "A silicone rubber mould of the heart," *Technol. Heal. care*, vol. 5, pp. 13–20, 1997.

_____

[14] G. D. Buckberg, A. Mahajan, B. Jung, and M. Markl, "MRI myocardial motion and fiber tracking : a confirmation of knowledge from different imaging modalities," *Eur. J. Cardio-Thoracic Surg.*, vol. 29, no. April, pp. 165–177, 2006.

[15] G. D. Buckberg, "The ventricular septum : the lion of right ventricular function , and its impact on right ventricular restoration," *Eur. J. Cardio-Thoracic Surg.*, vol. 29, no. April, pp. 272–278, 2006.

[16] S. K. Kohli, A. a Pantazis, J. S. Shah, B. Adeyemi, G. Jackson, W. J. McKenna, S. Sharma, and P. M. Elliott, "Diagnosis of left-ventricular non-compaction in patients with left-ventricular systolic dysfunction: time for a reappraisal of diagnostic criteria?," *Eur. Heart J.*, vol. 29, no. 1, pp. 89–95, Jan. 2008.

[17] S. E. Petersen, J. B. Selvanayagam, F. Wiesmann, M. D. Robson, J. M. Francis, R. H. Anderson, H. Watkins, and S. Neubauer, "Left ventricular non-compaction: insights from cardiovascular magnetic resonance imaging.," *J. Am. Coll. Cardiol.*, vol. 46, no. 1, pp. 101–5, Jul. 2005.

[18] S. Gati, N. Chandra, R. L. Bennett, M. Reed, G. Kervio, V. F. Panoulas, S. Ghani, N. Sheikh, A. Zaidi, M. Wilson, M. Papadakis, F. Carré, and S. Sharma, "Increased left ventricular trabeculation in highly trained athletes: do we need more stringent criteria for the diagnosis of left ventricular non-compaction in athletes?," *Heart*, vol. 99, no. 6, pp. 401–8, Mar. 2013.

[19] G. Captur, A. S. Flett, D. L. Jacoby, and J. C. Moon, "Left ventricular non-noncompaction: the mitral valve prolapse of the 21st century?," *Int. J. Cardiol.*, vol. 164, no. 1, pp. 3–6, Mar. 2013.

[20] D. Sedmera, T. Pexieder, M. Vuillemin, R. P. Thompson, and R. H. Anderson, "Developmental Patterning of the Myocardium," *Cell*, vol. 337, no. June 1999, pp. 319 –337, 2000.

[21] L. A. Taber and R. Perucchio, "Modeling Heart Development," *J. Elast. Phys. Sci. solids*, vol. 61, no. 1–3, pp. 165–197, 2001.

[22] G. Burch, "The trabeculae carneae--A thought," *Am. Heart J.*, vol. 89, no. 2, p. 261, 1975.

[23] G. E. Burch, C. T. Ray, and J. a. Cronvich, "The George Fahr Lecture: Certain Mechanical Peculiarities of the Human Cardiac Pump in Normal and Diseased States," *Circulation*, vol. 5, no. 4, pp. 504–513, Apr. 1952.

[24] L. J. J. Spreeuwers, S. J. J. Bangma, R. J. H. W. R. Meerwaldt, E. J. J. Vonken, and M. Breeuwer, "Detection of Trabeculae and Papillary Muscles in Cardiac MR Images," *Comput. Cardiol.*, pp. 415–418, 2005.

---

[25] K. L. Moore and A. M. R. Agur, *Essential clinical anatomy.* Lippincott Williams & Wilkins, 2007.

[26] G. Captur, V. Muthurangu, C. Cook, A. S. Flett, R. Wilson, A. Barison, D. M. Sado, S. Anderson, W. J. McKenna, T. J. Mohun, P. M. Elliott, and J. C. Moon, "Quantification of left ventricular trabeculae using fractal analysis.," *J. Cardiovasc. Magn. Reson.*, vol. 15, no. 1, p. 36, Jan. 2013.

[27] B. Moore and L. P. Dasi, "Multi-fractal nature of human left ventricular trabeculae: Possible biomechanical role?," *Chaos, Solitons & Fractals*, vol. 57, pp. 19–23, Dec. 2013.

[28] S. Kulp, M. Gao, S. Zhang, Z. Qian, S. Voros, D. Metaxas, and L. Axel, "Using High Resolution Cardiac CT Data to Model and Visualize Patient-Specific Interactions between Trabeculae and Blood Flow," *MICCAI 2011*, vol. 14, no. Pt 1, pp. 468–75, Jan. 2011.

[29] M. J. Bishop and G. Plank, "The role of fine-scale anatomical structure in the dynamics of reentry in computational models of the rabbit ventricles.," *J. Physiol.*, vol. 590, no. Pt 18, pp. 4515–35, Sep. 2012.

[30] M. J. Bishop, G. Plank, R. A. B. Burton, E. Schneider, D. J. Gavaghan, V. Grau, and P. Kohl, "Development of an anatomically detailed MRI-derived rabbit ventricular model and assessment of its impact on simulations of electrophysiological function," *Am J Physiol Hear. Circ Physiol*, vol. 298, pp. H699–H718, 2010.

[31] S. a Niederer and N. P. Smith, "At the heart of computational modelling.," *J. Physiol.*, vol. 590, no. Pt 6, pp. 1331–8, Mar. 2012.

[32] O. John, K. Kit, E. Kuhl, S. Göktepe, O. J. Abilez, and K. K. Parker, "A multiscale model for eccentric and concentric cardiac growth through sarcomerogenesis," *J. Theor. Biol.*, vol. 265, no. 3, pp. 433–442, Aug. 2010.

[33] N. P. Smith, D. P. Nickerson, E. J. Crampin, and P. J. Hunter, "Multiscale computational modelling of the heart," *Acta Numer.*, vol. 13, no. June 2004, p. 371, Jun. 2004.

[34] J. Wong, S. Göktepe, and E. Kuhl, "Computational modeling of chemo-electro-mechanical coupling : A novel implicit monolithic finite element approach," *Int. j. numer. method. biomed. eng.*, vol. 29, no. June, pp. 1104–1133, 2013.

[35] A. Krishnamurthy, C. T. Villongco, J. Chuang, L. R. Frank, V. Nigam, E. Belezzuoli, P. Stark, D. E. Krummen, S. Narayan, J. H. Omens, A. D. McCulloch, and R. C. P. C. Kerckhoffs, "Patient-Specific Models of Cardiac Biomechanics.," *J. Comput. Phys.*, vol. 244, pp. 4–21, Jul. 2013.

_____

[36]   T. B. Le and F. Sotiropoulos, "On the three-dimensional vortical structure of early diastolic flow in a patient-specific left ventricle.," *Eur. J. Mech. B. Fluids*, vol. 35, pp. 20–24, Jan. 2012.

[37]   M. P. Nash and P. J. Hunter, "Computational Mechanics of the Heart," *J. Elast.*, vol. 61, pp. 113–141, 2001.

[38]   J. D. Humphrey and F. C. Yin, "Constitutive relations and finite deformations of passive cardiac tissue II: stress analysis in the left ventricle," *Circ. Res.*, vol. 65, no. 3, pp. 805–817, Sep. 1989.

[39]   P. Lafortune, R. Arís, M. Vázquez, and G. Houzeaux, "Coupled electromechanical model of the heart: Parallel finite element formulation," *Int. j. numer. method. biomed. eng.*, vol. 28, pp. 72–86, 2012.

[40]   D. a Nordsletten, S. a Niederer, M. P. Nash, P. J. Hunter, and N. P. Smith, "Coupling multi-physics models to cardiac mechanics.," *Prog. Biophys. Mol. Biol.*, vol. 104, no. 1–3, pp. 77–88, Jan. 2011.

[41]   X. Zheng, J. H. Seo, V. Vedula, T. Abraham, and R. Mittal, "Computational modeling and analysis of intracardiac flows in simple models of the left ventricle," *Eur. J. Mech. - B/Fluids*, vol. 35, pp. 31–39, Sep. 2012.

[42]   L. a. Taber and W. W. W. Podszus, "A laminated shell model for the infarcted left ventricle," *Int. J. Solids Struct.*, vol. 34, no. 2, pp. 223–241, 1996.

[43]   M. Vendelin, P. H. M. Bovendeerd, J. Engelbrecht, and T. Arts, "Optimizing ventricular fibers: uniform strain or stress, but not ATP consumption, leads to high efficiency.," *Am. J. Physiol. Heart Circ. Physiol.*, vol. 283, no. 3, pp. H1072–81, Sep. 2002.

[44]   W. Kroon, T. Delhaas, T. Arts, and P. Bovendeerd, "Computational modeling of volumetric soft tissue growth: application to the cardiac left ventricle.," *Biomech. Model. Mechanobiol.*, vol. 8, no. 4, pp. 301–9, Aug. 2009.

[45]   P. H. M. Bovendeerd, W. Kroon, and T. Delhaas, "Determinants of left ventricular shear strain.," *Am. J. Physiol. Heart Circ. Physiol.*, vol. 297, no. 3, pp. H1058–68, Sep. 2009.

[46]   D. D. Streeter Jr., W. T. Hanna, and D. D. Streeter, "Engineering Mechanics for Successive States in Canine Left Ventricular Myocardium: I. cavity and wall geometry," *Circ. Res.*, vol. 33, no. 6, pp. 656–664, Dec. 1973.

[47]   J. H. Omens and Y. C. Fung, "Residual strain in rat left ventricle," *Circ. Res.*, vol. 66, no. 1, pp. 37–45, Jan. 1990.

_____

[48]   R. C. P. Kerckhoffs, P. H. M. Bovendeerd, J. C. S. Kotte, F. W. Prinzen, K. Smits, and T. Arts, "Homogeneity of Cardiac Contraction Despite Physiological Asynchrony of Depolarization: A Model Study," *Ann. Biomed. Eng.*, vol. 31, no. 5, pp. 536–547, May 2003.

[49]   W. Kroon, T. Delhaas, P. Bovendeerd, and T. Arts, "Computational analysis of the myocardial structure : Adaptation of cardiac myofiber orientations through deformation," *Med. Image Anal.*, vol. 13, no. 2, pp. 346–353, 2009.

[50]   P. H. M. Bovendeerd, T. Arts, J. M. Huyghe, D. H. van Campen, and R. S. Reneman, "Dependence of local left ventricular wall mechanics: a model study," *J Biomech.*, vol. 25, no. 10, pp. 1129–1140, 1992.

[51]   G. Tamborini, M. Pepi, F. Celeste, and M. Muratori, "Incidence and Characteristics of Left Ventricular False Tendons and Trabeculations in the Normal and Pathologic Heart by Second Harmonic Echocardiography," *J. Am. Soc. Echocardiogr.*, no. 1, pp. 367–374, 2004.

[52]   H. Lombaert, J.-M. Peyrat, P. Croisille, S. Rapacchi, L. Fanton, F. Cheriet, P. Clarysse, I. Magnin, H. Delingette, and N. Ayache, "Human atlas of the cardiac fiber architecture: study on a healthy population.," *IEEE Trans. Med. Imaging*, vol. 31, no. 7, pp. 1436–47, Jul. 2012.

[53]   D. A. Hooks, M. L. Trew, B. J. Caldwell, G. B. Sands, I. J. Legrice, and B. H. Smaill, "Laminar Arrangement of Ventricular Myocytes Influences Electrical Behavior of the Heart," *Circ. Res.*, vol. 101, no. 10, pp. 103–12, 2007.

[54]   W. Harvey, *Exercitatio Anatomica de Motu Cordis et Sanguinis in Animalibus.* 1628.

[55]   P. Helm, M. F. Beg, M. I. Miller, and R. L. Winslow, "Measuring and mapping cardiac fiber and laminar architecture using diffusion tensor MR imaging.," *Ann. N. Y. Acad. Sci.*, vol. 1047, pp. 296–307, Jun. 2005.

[56]   J. Chen, W. Liu, H. Zhang, L. Lacy, X. Yang, S. Song, S. A. Wickline, X. Yu, and X. Y. Re-, "Regional ventricular wall thickening reflects changes in cardiac fiber and sheet structure during contraction: quantification with diffusion tensor MRI," *Am. J. Physiol. Heart Circ. Physiol.*, vol. 289, no. 5, pp. 1898–1907, 2005.

[57]   I. Legrice, P. J. Hunter, and B. H. Smaill, "The architecture of the heart : a data-based model," *Society*, pp. 1217–1232, 2001.

[58]   G. A. Holzapfel, *Nonlinear solid mechanics.* John Wiley & Sons, Ltd, 2000.

_____

[59]   L. L. Demer and F. C. Yin, "Passive biaxial mechanical properties of isolated canine myocardium," *J. Physiol.*, vol. 339, no. June, pp. 615–630, 1983.

[60]   S. Dokos, B. H. Smaill, A. a Young, and I. J. LeGrice, "Shear properties of passive ventricular myocardium.," *Am. J. Physiol. Heart Circ. Physiol.*, vol. 283, no. 6, pp. H2650–9, Dec. 2002.

[61]   H. Ghaemi, K. Behdinan, and a D. Spence, "In vitro technique in estimation of passive mechanical properties of bovine heart part I. Experimental techniques and data.," *Med. Eng. Phys.*, vol. 31, no. 1, pp. 76–82, Jan. 2009.

[62]   F. C. Yin, "Ventricular wall stress," *Circ. Res.*, vol. 49, no. 4, pp. 829–842, Oct. 1981.

[63]   K. D. Costa, J. W. Holmes, A. D. Mcculloch, and T. H. E. Royal, "Modelling cardiac mechanical properties in three dimensions," *Philos. Trans. R. Soc. A Math. Phys. Eng. Sci.*, vol. 359, no. 1783, pp. 1233–1250, 2001.

[64]   G. a Holzapfel and R. W. Ogden, "Constitutive modelling of passive myocardium: a structurally based framework for material characterization.," *Philos. Trans. A. Math. Phys. Eng. Sci.*, vol. 367, no. 1902, pp. 3445–75, Sep. 2009.

[65]   V. Y. Wang, H. I. Lam, D. B. Ennis, B. R. Cowan, A. a Young, and M. P. Nash, "Modelling passive diastolic mechanics with quantitative MRI of cardiac structure and function.," *Med. Image Anal.*, vol. 13, no. 5, pp. 773–84, Oct. 2009.

[66]   J. Xi, P. Lamata, S. Niederer, S. Land, W. Shi, X. Zhuang, S. Ourselin, S. G. Duckett, A. K. Shetty, A. Rinaldi, D. Rueckert, R. Razavi, and N. P. Smith, "The estimation of patient-specific cardiac diastolic functions from clinical measurements.," *Med. Image Anal.*, vol. 17, no. 2, pp. 133–46, Feb. 2013.

[67]   M. a Hassan, M. Hamdi, and a Noma, "The nonlinear elastic and viscoelastic passive properties of left ventricular papillary muscle of a guinea pig heart.," *J. Mech. Behav. Biomed. Mater.*, vol. 5, no. 1, pp. 99–109, Jan. 2012.

[68]   T. C. Gasser, R. W. Ogden, and G. a Holzapfel, "Hyperelastic modelling of arterial layers with distributed collagen fibre orientations.," *J. R. Soc. Interface*, vol. 3, no. 6, pp. 15–35, Feb. 2006.

[69]   A. J. M. Spencer, *Constitutive Theory for Strongly Anisotropic Solids," , Continuum Theory of the Mechanics of Fibre-Reinforced Composites, CISM*

_____

Courses and Lectures No. 282, International Centre for Mechanical Sciences. A. J. M. Spencer (ed.), Springer-Verlag, Wien, 1984, pp. 1–32.

[70]   D. Westermann, M. Kasner, P. Steendijk, F. Spillmann, A. Riad, K. Weitmann, W. Hoffmann, W. Poller, M. Pauschinger, H.-P. Schultheiss, and C. Tschöpe, "Role of left ventricular stiffness in heart failure with normal ejection fraction.," *Circulation*, vol. 117, no. 16, pp. 2051–60, Apr. 2008.

[71]   S. Göktepe and E. Kuhl, "Electromechanics of the heart: a unified approach to the strongly coupled excitation–contraction problem," *Comput. Mech.*, vol. 45, no. 2–3, pp. 227–243, Nov. 2009.

[72]   L. a Taber, M. Yang, and W. W. Podszus, "Mechanics of ventricular torsion.," *J. Biomech.*, vol. 29, no. 6, pp. 745–52, Jun. 1996.

[73]   P. H. Backx, W. D. Gao, M. D. Azan-Backx, and E. Marban, "The relationship between contractile force and intracellular [Ca2+] in intact rat cardiac trabeculae.," *J. Gen. Physiol.*, vol. 105, no. 1, pp. 1–19, Jan. 1995.

[74]   L. R., *Tractatus de corde.* London UK: Oxford University Press, 1669.

[75]   G. Buckberg, J. I. E. Hoffman, N. C. Nanda, C. Coghlan, S. Saleh, and C. Athanasuleas, "Ventricular torsion and untwisting: further insights into mechanics and timing interdependence: a viewpoint.," *Echocardiography*, vol. 28, no. 7, pp. 782–804, Aug. 2011.

[76]   M. Takeuchi, Y. Otsuji, and R. M. Lang, "Evaluation of Left Ventricular Function Using Left Ventricular Twist and Torsion Parameters," *Curr. Cardiol. Rep.*, vol. 11, pp. 225–230, 2009.

[77]   F. Carreras, J. Garcia-Barnes, D. Gil, S. Pujadas, C. H. Li, R. Suarez-Arias, R. Leta, X. Alomar, M. Ballester, and G. Pons-Llado, "Left ventricular torsion and longitudinal shortening: two fundamental components of myocardial mechanics assessed by tagged cine-MRI in normal subjects," *Int. J. Cardiovasc. Imaging*, vol. 28, no. 2, pp. 273–284, Feb. 2011.

[78]   *Abaqus Documentation, version 6.10.* SIMULIA, Dessault systémes.

[79]   P. Bagnoli, N. Malagutti, D. Gastaldi, E. Marcelli, E. Lui, L. Cercenelli, M. L. Costantino, G. Plicchi, and R. Fumero, "Computational finite element model of cardiac torsion.," *Int J Artif Organs*, vol. 34, no. 1, pp. 44–53, 2011.

[80]   M. K. Sharp, "Development of a hydraulic model of the human systemic circulation.," *ASAIO J.*, vol. 45, pp. 535–540, 1999.

_____

[81]   L. N. Katz and H. S. Feil, "Observations on the dynamics of ventricular systole. I Auricolar Fibrillation.," *Arch. Int. Med.*, vol. 32, no. 5, pp. 672–692, 1923.

[82]   C. M. Quick, D. S. Berger, and A. Noordergraaf, "Apparent arterial compliance.," *Am. J. Physiol. - Hear. Circ. Physiol.*, vol. 274, pp. H1393–H1403, 1998.

[83]   C. P. Appleton, "Influence of incremental changes in heart rate on mitral flow velocity: assessment in lightly sedated, conscious dogs.," *J. Am. Coll. Cardiol.*, vol. 17, no. 1, pp. 227–36, Jan. 1991.

[84]   B. Jung, M. Markl, D. Fo, D. Föll, and J. Hennig, "Investigating myocardial motion by MRI using tissue phase mapping.," *Eur. J. Cardiothorac. Surg.*, vol. 29 Suppl 1, pp. S150–7, May 2006.

[85]   B. Jung, D. Föll, P. Böttler, S. Petersen, J. Hennig, and M. Markl, "Detailed analysis of myocardial motion in volunteers and patients using high-temporal-resolution MR tissue phase mapping.," *J. Magn. Reson. Imaging*, vol. 24, no. 5, pp. 1033–9, Dec. 2006.

[86]   P. P. Sengupta, a J. Tajik, K. Chandrasekaran, and B. K. Khandheria, "Twist mechanics of the left ventricle: principles and application.," *JACC. Cardiovasc. Imaging*, vol. 1, no. 3, pp. 366–76, May 2008.

[87]   Y. Notomi, Z. B. Popovic, H. Yamada, D. W. Wallick, M. G. Martin, S. J. Oryszak, T. Shiota, N. L. Greenberg, and J. D. Thomas, "Ventricular untwisting: a temporal link between left ventricular relaxation and suction.," *Am. J. Physiol. Heart Circ. Physiol.*, vol. 294, no. 1, pp. H505–13, Jan. 2008.

[88]   A. A. Young and B. R. Cowan, "Evaluation of left ventricular torsion by cardiovascular magnetic resonance.," *J. Cardiovasc. Magn. Reson.*, vol. 14, p. 49, Jan. 2012.

[89]   E. Marcelli, L. Cercenelli, M. Parlapiano, R. Fumero, P. Bagnoli, M. L. Costantino, and G. Plicchi, "Effect of right ventricular pacing on cardiac apex rotation assessed by a gyroscopic sensor.," *ASAIO J.*, vol. 53, no. 3, pp. 304–9, 2007.

[90]   B. M. Van Dalen, O. I. I. Soliman, W. B. Vletter, F. J. Cate, and M. L. Geleijnse, "Age-related changes in the biomechanics of left ventricular twist measured by speckle tracking echocardiography," *Am J Physiol Hear. Circ Physiol*, vol. 295, pp. 1705–1711, 2008.

[91]   N. B. Ingels, "Myocardial fiber architecture and left ventricular function.," *Technol. Health Care*, vol. 5, no. 1–2, pp. 45–52, Apr. 1997.

_____

[92]   T. Arts, R. S. Reneman, and P. C. Veenstra, "a model of the mechanics of the left ventricle.pdf," *Ann. Biomed. Eng.*, vol. 7, pp. 299–318, 1979.

[93]   E. Nagel, "Cardiac rotation and relaxation in patients with aortic valve stenosis," *Eur. Heart J.*, vol. 21, no. 7, pp. 582–589, Apr. 2000.

[94]   L. K. Waldman, Y. C. Fung, and J. W. Covell, "Transmural myocardial deformation in the canine left ventricle. Normal in vivo three-dimensional finite strains.," *Circ. Res.*, vol. 57, no. 1, pp. 152–63, Jul. 1985.

[95]   J. Wang, D. S. Khoury, Y. Yue, G. Torre-amione, and S. F. Nagueh, "Preserved left ventricular twist and circumferential deformation, but depressed longitudinal and radial deformation in patients with diastolic heart failure.," *Eur. Heart J.*, vol. 29, no. 10, pp. 1283–9, May 2008.

[96]   K. Kindberg, M. Karlsson, N. B. Ingels, and J. C. Criscione, "Nonhomogeneous strain from sparse marker arrays for analysis of transmural myocardial mechanics.," *J. Biomech. Eng.*, vol. 129, no. 4, pp. 603–10, Aug. 2007.

[97]   F. E. Rademakers, W. J. Rogers, W. H. Guier, G. M. Hutchins, C. O. Siu, M. L. Weisfeldt, J. L. Weiss, and E. P. Shapiro, "Relation of regional cross-fiber shortening to wall thickening in the intact heart. Three-dimensional strain analysis by NMR tagging," *Circulation*, vol. 89, no. 3, pp. 1174–1182, Mar. 1994.

[98]   M. S. Suffoletto, K. Dohi, M. Cannesson, S. Saba, and J. Gorcsan, "Novel speckle-tracking radial strain from routine black-and-white echocardiographic images to quantify dyssynchrony and predict response to cardiac resynchronization therapy.," *Circulation*, vol. 113, no. 7, pp. 960–8, Feb. 2006.

[99]   S. Langeland, J. D'hooge, P. F. Wouters, H. A. Leather, P. Claus, B. Bijnens, and G. R. Sutherland, "Experimental validation of a new ultrasound method for the simultaneous assessment of radial and longitudinal myocardial deformation independent of insonation angle.," *Circulation*, vol. 112, no. 14, pp. 2157–62, Oct. 2005.

[100]   K. May-Newman, J. H. Omens, R. S. Pavelec, and a. D. McCulloch, "Three-dimensional transmural mechanical interaction between the coronary vasculature and passive myocardium in the dog," *Circ. Res.*, vol. 74, no. 6, pp. 1166–1178, Jun. 1994.

[101]   J. H. Omens, K. D. May, and A. D. McCulloch, "Transmural distribution of three-dimensional strain in the isolated arrested canine left ventricle.," *Am. J. Physiol.*, vol. 261, no. 30, pp. H918–H928, 1991.

_____

[102]   T. Arts, P. Bovendeerd, T. Delhaas, and F. Prinzen, "Modeling the relation between cardiac pump function and myofiber mechanics," *J. Biomech.*, vol. 36, no. 5, pp. 731–736, May 2003.

[103]   A. C. Burton, *Physiology and Biophysics of the Circulation: an introductory text.* Year Book Medical Publishers, 1972.

[104]   H. Suga, T. Hayashi, and M. Shirahata, "Ventricular systolic pressure-volume area as predictor of cardiac oxygen consumption.," *The American journal of physiology*, vol. 240, no. 1. pp. H39–44, Jan-1981.

[105]   D. S. Loiselle, E. J. Crampin, S. a Niederer, N. P. Smith, and C. J. Barclay, "Energetic consequences of mechanical loads.," *Prog. Biophys. Mol. Biol.*, vol. 97, no. 2–3, pp. 348–66, 2008.

[106]   R. Fumero, F. M. Montevecchi, and U. F. Tesler, *La circolazione assistita e il cuore artificiale.* Ricrodati/ Industria Chimica e Farmaceutica s.a.s., 1968.

[107]   R. R. Nelson, F. L. Gobel, C. R. Jorgensen, K. Wang, Y. Wang, and H. L. Taylor, "Hemodynamic Predictors of Myocardial Oxygen Consumption During Static and Dynamic Exercise," *Circulation*, vol. 50, no. 6, pp. 1179–1189, Dec. 1974.

[108]   J. Vinten-Johansen and V. H. Thourani, "Myocardial protection: an overview.," *J. Extra. Corpor. Technol.*, vol. 32, no. 1, pp. 38–48, Mar. 2000.

[109]   S. J. Sarnoff, E. Braunwald, G. H. Welch, R. B. Case, W. N. Stainsby, and R. Macruz, "Hemodynamic Determinants of Oxygen Consumption With Special Reference to the Tension-Time Index," *Heart*, no. May, 1957.

[110]   A. Redaelli, F. Maisano, M. Soncini, O. Alfieri, and F. M. Montevecchi, "Haemodynamics and mechanics following partial left ventriculectomy: a computer modeling analysis," *Med. Eng. Phys.*, vol. 26, no. 1, pp. 31–42, Jan. 2004.

[111]   W. J. Paulus, C. Tschöpe, J. E. Sanderson, C. Rusconi, F. a Flachskampf, F. E. Rademakers, P. Marino, O. a Smiseth, G. De Keulenaer, A. F. Leite-Moreira, A. Borbély, I. Edes, M. L. Handoko, S. Heymans, N. Pezzali, B. Pieske, K. Dickstein, A. G. Fraser, and D. L. Brutsaert, "How to diagnose diastolic heart failure: a consensus statement on the diagnosis of heart failure with normal left ventricular ejection fraction by the Heart Failure and Echocardiography Associations of the European Society of Cardiology.," *Eur. Heart J.*, vol. 28, no. 20, pp. 2539–50, Oct. 2007.